Conceptual Design Optimisation of a Flying V Aircraft

T.A. Nieuwenhuizen

Delft University of Technology

TU Delft

Conceptual Design Optimisation of a Flying V Aircraft

by

T.A. Nieuwenhuizen

to obtain the degree of Master of Science
at the Delft University of Technology,
to be defended publicly on Monday August 30, 2021 at 13:00.

Student number:	4148495	
Project duration:	March, 2020 – August, 2021	
Thesis committee:	Prof. em. Dr.-Ing. G. Eitelberg,	TU Delft, Chairman
	Dr. ir. R. Vos,	TU Delft, Supervisor
	Dr. ir. D. Peeters,	TU Delft
	Dipl. Ing. K. Bender,	Airbus

TU Delft

Summary

In the past decades, there has been an increasing awareness of the need for more environmentally-friendly passenger aircraft. The lack of a feasible roadmap to carbon-neutral air traffic, especially for long-range flights, using the traditional tube-and-wing form factor shows that a disruptive technology is necessary to bridge this gap. The Flying V is a newly proposed aircraft configuration which promises to enable a leap in long-range passenger aircraft efficiency. Integration of passengers and cargo within the wing allows for a design which is more efficient both aerodynamically thanks to the lack of the non-lifting fuselage, and structurally since the weight is distributed more in line with the lift distribution, reducing the need for long load-paths.

This study aims to evaluate the entire Flying V concept, integrating several disciplines. Building on the lessons learned from previous in-depth studies into the separate disciplines, a performance model is constructed for the overall aircraft, resulting in an estimate of important characteristics of the complete aircraft, mainly a 31% decrease in mission fuel burn compared to the latest generation of long-range conventional aircraft with a maximum takeoff weight reduction of 21%.

Subsequently, a design optimisation aimed at minimising mission fuel burn is executed using the developed performance model, resulting in an updated design for the Flying V concept achieving a 35% decrease in mission fuel burn with a reduction in maximum takeoff weight of 25% compared to the same conventional aircraft.

This optimised design features a narrower but longer cabin as compared to the baseline Flying V, which necessitates a modified cabin layout with 9-abreast seating in a 3-3-3 configuration instead of the 10-abreast 3-4-3 configuration of the baseline. This adjustment distributes the payload over the span to a greater extent, improving the match between the lift and weight distributions.

Additionally, the sweep of the inner wing is decreased, with the constraint on both inner and outer wing sweep active. This shows that the wave drag of this configuration on both the inner and the outer wing is an important aspect of this design in terms of impact on the mission performance.

Preface

Dear reader,

This thesis marks the completion of my studies of Aerospace Engineering at Delft University of Technology. The Flying V concept has been an exciting subject to immerse myself in for this final project, since it has given me an opportunity to work on something truly innovative, and to experience and overcome all the uncertanties that invariably accompany such new technology. It was equally exciting to find that the concept does indeed have a great potential and I am very curious to see where the project will go from here.

I would like to thank dr. Roelof Vos for his guidance and support during this project. It has been very interesting to discuss the intricacies of aircraft design, and of unconventional aircraft design in particular, during our meetings.

Finally, a well-deserved thanks goes out to my parents and my girlfriend. To my parents for their unwavering support and belief in my success throughout the past years. To my girlfriend for her extensive help and motivation in reaching this point.

Ties Nieuwenhuizen
Delft, August 2021

Contents

Nomenclature

A Aspect ratio [-].

C_D Drag coefficient [-].

C_L Lift coefficient [-].

C_{D_0} Zero-lift drag coefficient [-].

M Mach number [-].

S Reference area [m^2].

T Thrust [N].

$V_{\mathbf{A}}$ Manoeuvre speed.

$V_{\mathbf{C}}$ Cruise speed.

$V_{\mathbf{D}}$ Dive speed.

$V_{\mathbf{S}}$ Stall speed.

W Weight [N].

Λ Sweep angle [°].

$\delta_{\mathbf{f}}$ Maximum flap deflection.

$\frac{L}{D}$ Lift-to-drag ratio [-].

$\frac{t}{c}$ Thickness-to-chord ratio [-].

λ Taper ratio.

$\vec{x}$ Design vector [-].

$\widehat{\text{FV}}$ Flying V configuration used in FEM analysis.

b Span [m].

e Oswald efficiency factor [-].

$u_{\mathbf{ult}}$ Ultimate load factor.

$w''_{\mathbf{st}}$ Secondary structure weight.

$w'_{\mathbf{st}}$ Primary structure weight.

$w_{\mathbf{st}}$ Structure weight.

w_i Weight after mission segment i.

List of Figures

List of Tables

1

Introduction

The modern jet transport aircraft are true marvels of engineering, transporting hundreds of passengers over thousands of miles in a timespan of mere hours. Aircraft have come a long way since the start of aviation, with significant improvements in multiple disciplines. In materials, what started as wood and fabric construction has evolved through increasingly strong metal alloys to current aircraft constructed largely from composites. In aerodynamics, aircraft have progressed from braced bi-planes to cleaner configurations producing less drag, to high-subsonic aircraft with supercritical airfoils and swept wings and even to super- and hypersonic concepts. Throughout this time, propulsion technology has kept pace, moving from heavy piston-propeller concepts via powerful but fuel-hungry turbojets to today's highly efficient high bypass-ratio turbofan engines.

Yet, there has been an unchanging factor in transport aircraft throughout this time. Following the principles of George Cayley, the functions of lift, propulsion, stability and control, and carrying payload have been carried out by distinctly separate components: wings, engines, tail surfaces and a fuselage. There is, however, incentive to reconsider this paradigm.

In the past decades it has become increasingly clear that there is a discrepancy between the ever-increasing growth in air traffic, which despite the short-term impact of the Covid-19 pandemic, shows no signs of levelling off in the long un, on the one hand, and the growing concern over the adverse environmental impact of flying on the other hand. While carbon-neutral solutions in many fields are nearing maturity and are being deployed already, such as electric cars in combination with solar, wind and nuclear electricity production, there is no such feasible roadmap for the near future in aviation. Especially long-range transport aircraft face tremendous challenges in this respect due to their stringent weight and power requirements.

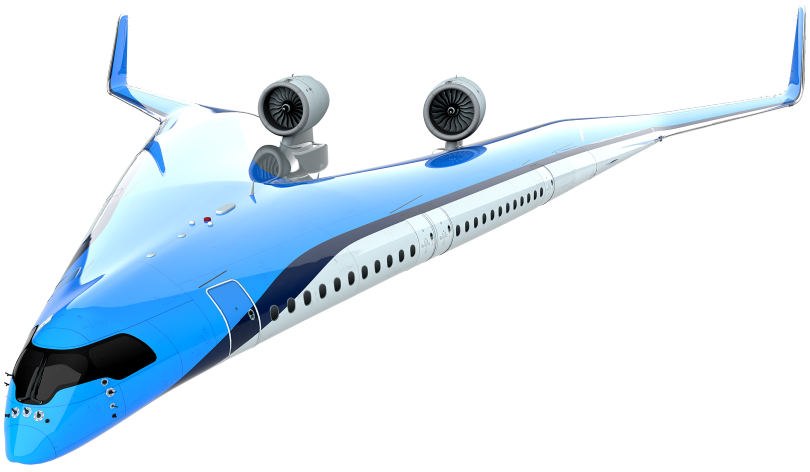

Figure 1.1: Artist impression of the Flying V concept [1]

Therefore, there has been an increased effort in recent years to develop radically new concepts which have the potential of making a significant positive impact on the emissions of aircraft. These concepts challenge Cayley's principles by attempting to integrate many of the functions currently fulfilled by different components of an aircraft. The aim is to increase efficiency of the concept as a whole by reducing the weight and drag penalties associated with more components.

One of the most promising of these concepts is the Flying V, proposed by Benad [1]. This concept features two tubular, pressurised cabins joined together in a V shape carrying the passengers, cargo, and fuel within the wing. The removal of the need for a fuselage improves the aerodynamic efficiency, as well as distributing the weight of the payload over the wing, shortening load paths from lift to payload. The highly-swept inner wing allows for the structurally efficient elliptical cabins to be fitted inside without an excessive increase in wave drag associated with thick airfoils. An artist impression of the concept can be seen in Figure 1.1.

Further research into a wide range of topics with regard to the Flying V concept has been performed in the past years at TU Delft. With the increased knowledge about the Flying V concept gathered in these previous studies, it is now possible to analyse the entire concept and refine it to find improvements where possible.

1.1. Research Objective and Questions

This study aims to construct an aircraft performance model based on research into the Flying V, which can both be used to evaluate the current concept and compare it to the state-of-the-art in long-range passenger air travel, and to optimise the conceptual design in regard to the mission fuel efficiency to find possible avenues for further performance improvements.

The research questions of this study are therefore:

- What is the mission performance of the Flying V when integrating results from previous analyses into a single aircraft model?
- What are possible improvements to the Flying V concept with respect to the mission performance?

1.2. Report Outline

Before going into the specifics of the method used to answer the research questions, chapter 2 provides an overview of background information regarding the Flying V and related concepts, as well as a review of previous work regarding the Flying V. Next, chapter 3 describes the methods used in building the aircraft performance model and the setup of the performance optimisation. Chapter 4 discusses the steps taken to ensure the validity of the developed model. Results from the performance model evaluation as well as results for the optimisation and the ensuing configuration are presented in chapter 5. Finally, the conclusions drawn from this research and recommendations for further study can be found in chapter 6.

[1] Image source https://www.tudelft.nl/en/ae/flying-v/

2

Background

This chapter aims to provide the background information for this study, starting with a description of the flying wing and related concepts. Subsequently, the Flying V specifically is discussed, including different research performed for this concept, with a focus on research used in this study.

2.1. Flying Wings and Blended-Wing-Bodies

This section presents the current state of research on the subject of the Flying V and related concepts, as well as additional background information relevant to the current research.

The flying wing and Blended Wing Body (BWB) are concepts for aircraft focused on maximising both aerodynamic and structural efficiency by integrating the functions of creating aerodynamic lift and carrying payload into a simple whole. A pure flying wing consists of solely a wing, while a BWB has a distinct fuselage shape which is smoothly integrated with the wings, and usually produces some amount of lift. See Figure 2.1 for examples of both.

(a) Example of a flying wing: the YB-49 bomber concept [1]

(b) Example of a BWB [2]

Figure 2.1: Examples of flying wing and BWB aircraft

2.1.1. Historical Context

The concept of a flying wing aircraft, and by extension the BWB and related concepts, have been studied in different ways at different times in history. One of the first functioning large-scale flying wings to be built was the YB-35 developed by Northrop in the 1940s, later developed into the YB-49 [3]. Since the main goal of this prototype bomber was to carry out bombing missions over Germany from mainland United States, extraordinarily long range for its time was a driving requirement in the design. The solution as proposed by Northrop was to remove as much drag-creating parts of the aircraft such that all exposed skin was contributing to lift, hence improving the lift-to-drag ratio ($\frac{L}{D}$) and leading to an

[1] Image source: https://commons.wikimedia.org/wiki/File:YB49-2_300.jpg

all-wing design. Although the expected range of the concept was promising, the project was plagued by a combination of political and performance problems leading to its cancellation. The two main problems with performance were poorly damped yaw, requiring sophisticated autopilots for accurate bombing, and a design cruise speed which was overtaken by the increasing speed demands driven by the introduction of the jet engine.

The flying wing concept saw little development in the following decades, for a more thorough look into the historical developments the reader is redirected to a paper by Okonkwo [4]. More recently however, interest in the concept has been renewed with several projects in different parts of the world. Focus since then has been mostly on the BWB concept, and less on pure flying wings. An extensive overview of BWB developments is presented by Chen et al. [5].

2.1.2. Overview of Notable Projects

One of the most notable developments was carried out at the McDonnell Douglas and Boeing companies, funded by NASA Langley [6]. Carried out from 1993 to about 2002, the study consisted of three major iterations of a large scale BWB passenger transport with an initial projected capacity of 800 passengers and a 7000-nmi range, later adjusted to 450 passengers. In the course of the project these teams investigated a wide variety of aspects of the concept, including but not limited to stability and control, structure, trim, and passenger comfort. In addition, a multidisciplinary design optimisation (MDO) framework was developed and used to optimise the design. In conclusion, Liebeck notes a possible 18% reduction in take-off weight and 32% reduction in fuel burn per seat mile when compared to the A380-700 [6].

It should be noted that the concepts in Liebecks paper were designed for cruise Mach numbers of 0.85 to 0.95, which by today's standards is relatively high, indicating that not all aerodynamic conclusions from this paper are valid for concepts that might be currently considered. Additionally, Liebeck assumes it to be acceptable for the aircraft to be statically unstable. While this may lead to higher cruise efficiency, the current certification specifications [7] do not allow for this characteristic, and expecting these regulations to change can be a large risk. This means that the results noted may not be achievable in practice.

A study into the stability of BWB was performed by Ammar [8] who considers the design of a somewhat smaller, 200 passenger aircraft. Using a low-fidelity MDO approach a design optimised for a combination of maximum take-off weight (MTOW) and lift-to-drag ratio is found and subsequently analysed for performance and (dynamic) stability. While it finds a positive longitudinal stability, a lateral instability in the Dutch-Roll mode in particular is found to be present.

The relaxed requirements on stability in Liebeck [6] and the result of lateral instability by Ammar [8] indicate that stability is an important factor in the design of a flying wing or Blended Wing Body (BWB) aircraft.

Around the same time as the work described by Liebeck, the Central Aerohydrodynamic Institute (TsAGI) in Russia performed an investigation into an ultra-high capacity flying wing-type aircraft [9]. In this paper, several concepts for a mission of 750 passengers over 13,700km at mach 0.85 were discussed. The main contenders were a hybrid or integrated-wing-body (IWB), a lifting-body, and pure flying wing concept. The IWB utilises a conventional but shortened fuselage with an enlarged centre-wing section which can also house passengers. The lifting-body configuration consists of a wide, airfoil shaped fuselage combined with a regular wing. The ”pure” flying wing concept, although more pure flying wing than Boeings concepts presented by Liebeck, still resembles a BWB somewhat due to its large centre-wing chords.

Following an investigation into the efficiency of the configurations in terms of fuel efficiency and weight it is concluded that the IWB is the best concept for this mission. It should be noted, however, that this comparison was driven in a large part by the excessive wave-drag caused by the thicker airfoil sections of the flying wing and lifting-body concepts. Therefore, it stands to reason that, should a solution for the mitigation of this wave drag be found or the cruise speed requirement be relaxed, the conclusion may change.

Another notable work in terms of configuration is the concept investigated by Martinez-Val in his papers [10, 11]. A unique aspect of this concept is what he calls the ”C-flying wing” configuration. In this configuration, atop large winglet-type vertical surfaces at the wingtips additional, smaller, horizontal winglets are added, see Figure 2.2. This c-shaped wing configuration was first proposed by McMasters [12], who presents it as a way of both increasing span efficiency factor and to obtain an alternative

for the horizontal tail, as the sweep of both the main wing and the vertical part of the winglet causes it to be positioned well aft of the centre of gravity.

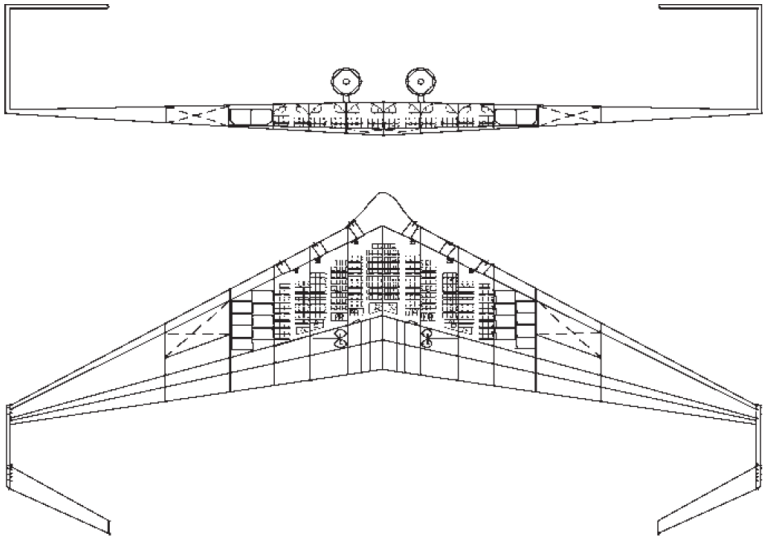

Figure 2.2: Sketch showing the ”C-flying wing configuration”, top and front views [10]

In the past decade, a notable continuation of the work described above has been proposed as a way to reach NASA New Aviation Horizons N+2 goals [2, 13], where a BWB is considered as a possibility for reaching more sustainable aviation. Lastly, it should be noted that BWB concepts are also being applied in the unmanned aviation field, such as by Panagiotou et al. [14].

2.1.3. Flying V

The Flying V concept is proposed by Benad [1] as a way to achieve a high-capacity pure flying wing passenger transport aircraft while reducing the challenges traditionally associated with flying wings and BWBs. The two main challenges addressed by this configuration are the structural challenge of pressurising a non-cylindrical cabin and the issue of fitting the payload (i.e. passengers) into the wing while maintaining a sufficiently thin airfoil section to prevent excessive transonic drag.

In order to solve the structural challenge, Benad’s concept employs two cylindrical, pressurised sections for the payload, leading to a considerably simplified structural design when compared to, e.g. the designs presented by Liebeck [6]. In a later work by Faggiano et al. [15], an alteration was proposed to this concept, adopting the cylindrical cabin concept proposed by Vos et al. [16].

To prevent the issue of excessive transonic drag due to thick airfoil sections, Benad proposes to employ high sweep for the two pressurised cabins, leading to a streamwise cross-section of a lower thickness-to-chord ratio. The outer wings extending beyond the pressurised sections were to have a much lower sweep angle, see Figure 2.3. This sweep angle, too, was later adjusted by Faggiano [15] to a higher sweep in order to prevent excessive wave drag on the outer wing.

Two important additional features of the Flying V are presented by Benad. The first being the placement of the engines above the wing which would provide noise shielding and thus reduced engine noise reaching the ground. The second is the wing area being sufficiently large to remove the need for high-lift devices (HLDs), thus removing complexity from the aircraft both in the amount of moving parts, and in the complexity of trimming a tail-less aircraft with deployed HLDs. In later research in a windtunnel [17], it was found that the high-sweep inner wing also produces vortex lift at high angles of attack, increasing the stall angle of attack.

Since the introduction of the Flying V concept by Benad, extensive research has been performed into this concept at TU Delft. The studies into the aerodynamic and structural analyses will be explored in more detail in the following sections since they are the starting point for the performance model in this study. Beside these disciplines, studies were performed on engine-airframe integration [18], a study using windtunnel data for aerodynamic model identification [19], a study on the influence of ground

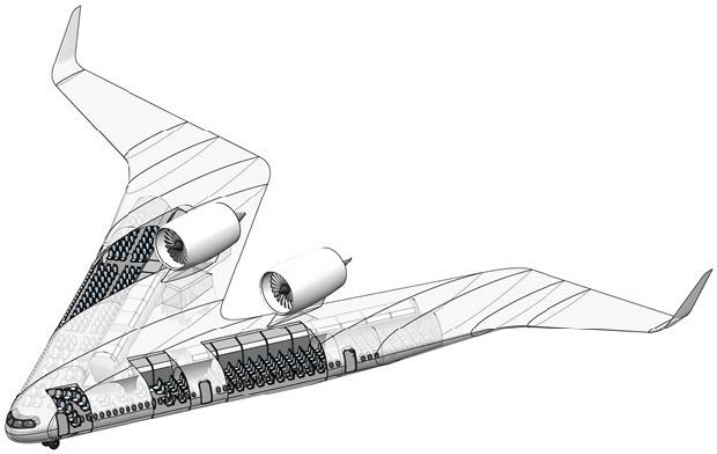

Figure 2.3: The Flying V concept as proposed by Benad [1]

effect [20] and an investigation into the stability and control of a scaled model [21]. An investigation into the feasibility of a family of Flying V aircraft has been performed by Oosterom [22]. Additionally, studies into the winglet integration [23, 24], landing gear [25] and cockpit design [26] have been performed.

2.2. Aerodynamics

An essential part of the design and analysis of any aircraft is the aerodynamics. For the current project it is necessary to investigate the latest knowledge of the aerodynamics of both the Flying V and a conventional reference aircraft, to enable a representative comparison. For the aerodynamics of the Flying V, research was limited to the work performed for the actual Flying V project, as any work on similar projects, however interesting, cannot be applied to the current project as for the performance model data is required specific to this concept.

2.2.1. Overview of Work on the Flying V

As mentioned in subsection 2.1.3, work on the Flying V aerodynamics was started by Benad in his paper introducing the concept [1]. This analysis on the initial concept used a vortex lattice method which was unable to predict any wave drag. This analysis is not of practical use currently, both because of the low-fidelity method used and because the aerodynamic design of the concept has since been altered. This alteration is described by Faggiano et al. [15]. The main modification is the increase in sweep for the outer wings, i.e. the part outboard of the kink., see Figure 2.4. The modification described in this paper and the corresponding thesis [27] was supported by an Euler solver analysis combined with an empirical method for profile drag. This allows the authors to obtain a much higher-fidelity estimate of the aerodynamic characteristics of the aircraft than Benad in his work, as well as employing optimisation algorithms to optimise the aerodynamic shape.

The work of Faggiano is a suitable starting point in collecting aerodynamic data on the Flying V concept, finding an $\frac{L}{D}$ of 23.7 and a C_{D_0} of 57 counts, based on a reference area of 883.3m^2. Following this work, wind tunnel testing on a scaled model of the Flying V was performed by Viet [17] and Ruiz García [19]. The work by Viet focuses on the (mostly qualitative) aerodynamic flow characteristics, stall behaviour and static stability. Ruiz García's work consists of developing a complete state-space model of the Flying V scale model, including a trim routine.

The work by Viet is useful mostly in the low-speed aspects of the flight, mainly take-off and landing performance analysis, where the high angle of attack data, especially maximum lift coefficient, is useful to determine e.g. the minimum approach speed. One of the main important findings in this work is that the limiting factor on the minimum speed is not loss of lift, but rather a negative stability at high angles of attack, limiting the practical operational regime. A further investigation into this unstable pitch break was conducted by van Uitert [28], also investigating aerodynamic add-ons to partially mitigate this effect,

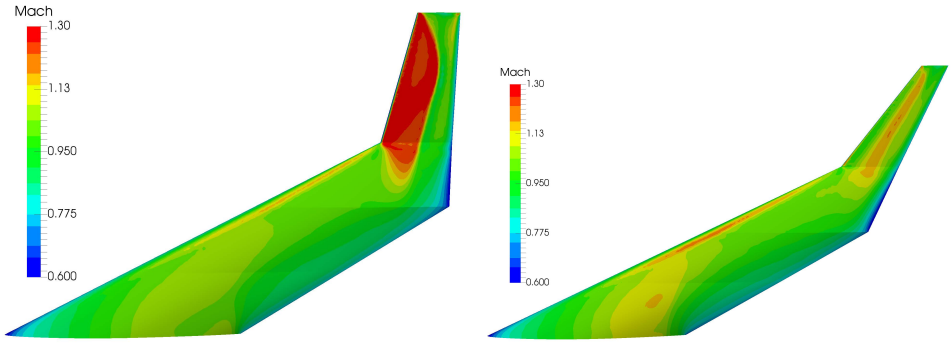

(a) Baseline configuration (b) Optimised configuration

Figure 2.4: Alteration of the aerodynamic concept by Faggiano [15]

leading to an updated maximum useful lift coefficient.

2.2.2. Models for the Conventional Aircraft

Next to the data for the Flying V, representative data must also be found for the conventional reference concept for comparison. Although there is ample information on the aerodynamics of tube-and-wing aircraft, detailed data for the A350-900 reference aircraft is not available, as any such data is kept confidential by Airbus.

Therefore, an alternative is found in the NASA Common Research Model (CRM) [29]. This model was developed by NASA as a reference for the validation of Computational fluid dynamics (CFD) codes. As such, the model was designed to resemble a modern transport aircraft as much as possible. This design was then extensively tested in multiple wind tunnels to obtain as objective a set of data as possible.

2.3. Structural Design and Weight Estimation

The second important discipline in the design and analysis of an aircraft is the structural design, and closely associated with it the estimation of aircraft weight. In order to be able to determine the amount of fuel burnt during a mission, knowing the Operational empty weight (OEW) is essential.

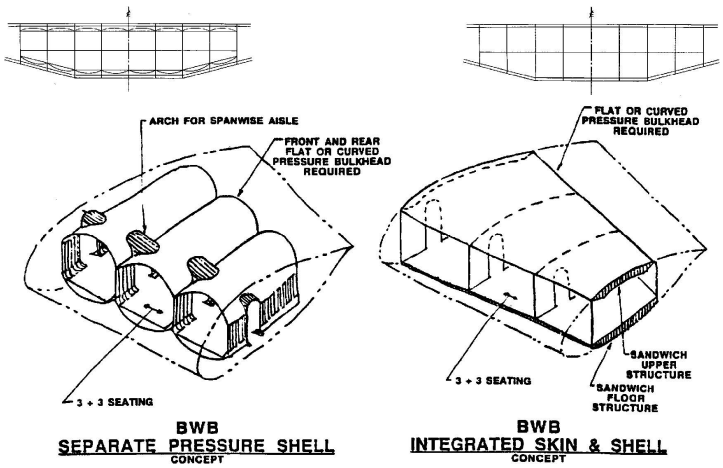

Figure 2.5: Pressure vessel structural concepts as proposed by Liebeck [6]

2.3.1. Structural Design of the Flying V

The structural design concept of the Flying V as proposed by Benad [1] was focused on cylindrical cabin cross sections put at an angle to the freestream flow. Benad proposed two such cylinders, one for the passenger cabin and one for the cargo, see Figure 2.6a. This configuration was aimed at struc-

tural efficiency of the pressurised parts of the aircraft, since a cylinder naturally carries pressurisation loads well through hoop stresses. This is contrasted by the relatively complex pressure vessel structural concepts discussed by Liebeck [6], where an air-matress like structure and a loaded sandwich construction skin were proposed, see Figure 2.5.

In the work of Faggiano et al. [15], an alteration is proposed based on the work by Vos et al. [16], where the two cylindrical cross-sections are replaced by one elliptical cross-section. Although this solution is structurally less efficient than the cylinders since an elliptical cross-section is naturally less well-suited to carry pressurisation loads, it was preferred for both the improved design flexibility it offers, enabling the development of an improved aerodynamic design, and the more efficient use of space within the wing. The new concept is shown in Figure 2.6b.

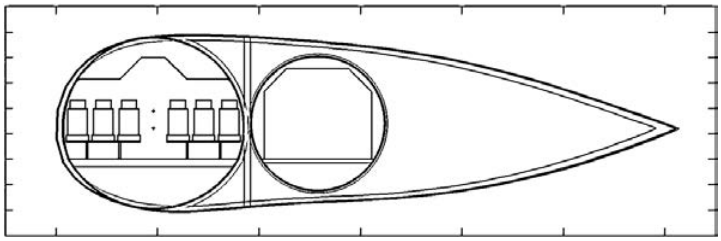

(a) Structural concept as proposed by Benad in cross-sectional view perpendicular to the cabin [1]

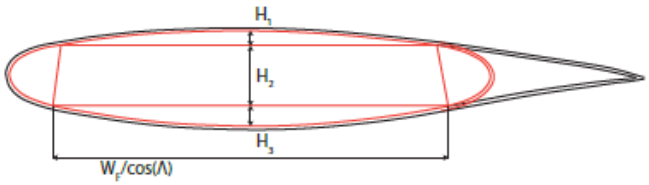

(b) Structural concept as proposed by Faggiano in streamwise cross-sectional view [15]

Figure 2.6: Comparison of structural concepts by Benad and Faggiano

The oval-cabin design was expanded upon by van der Schaft [30] and Claeys [31], who also consider more three-dimensional aspects beyond the cross-section, such as transitions between sections and placement of structural components. This design features a taper in the aft part of the pressurised cabin to ensure a fit within the aerodynamic design of the outer mold, see Figure 2.7.

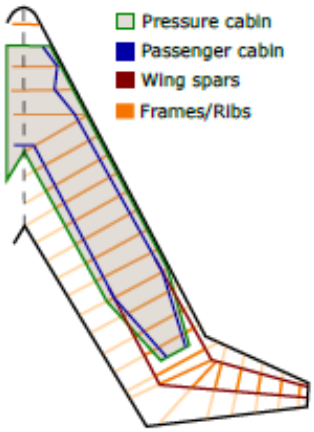

Figure 2.7: Top view of the structural concept developed by van der Schaft [30]

2.3.2. Weight Estimation

The work by Claeys [31] provides a finite element method (FEM) analysis on both a conventional aircraft and the Flying V, based on the structural concept developed by van der Schaft [30]. Although

FEM weight is not total structure weight, this provides a good starting point for a representative weight estimation of the Flying V, finding a FEM weight of 24.7t for the Flying V and 29.8t for a reference tube-and-wing configuration, both based on a MTOW of 260t, giving a reduction in FEM weight of 17%. A lower fidelity, but still physics-based, structure weight analysis for the inner wing structure, mainly the oval fuselage, was developed by Oosterom [22]. The combination of data from these studies provides sufficient basis for a representative structure weight estimation.

For conventional aircraft, more established methods are used, such as Class II weight estimation methods. The method used in this study is the Torenbeek method [32]. The method divides the aircraft into parts and systems in order to use empirical relations to estimate the component masses of each part or system. Because of this subdivision it is also possible to employ parts of this method for the estimation of system and component weights of the Flying V for systems and components whose weight is not dependent on the changes in concept between the conventional aircraft and the Flying V.

3

Methodology

To find where improvements to the existing Flying V concept are possible, multidisciplinary design optimisation (MDO) is employed. This method integrates all the analyses used in the various disciplines involved in a product into a single automated design loop, to which an optimisation algorithm can then be applied to find the design which is best suited to the specified objectives.

To aid in the process of integration, the knowledge based engineering (KBE) platform ParaPy[1] is used. This platform provides the functionality to construct a central product model which can be used as input to all the discipline analyses, which ensures consistency between them. This product model consists of the aircraft geometry, but also other system characteristics such as the weight and engine thrust. An overview of the complete analysis including optimisation can be found in Figure 3.1.

Because optimisation algorithms require many evaluations of the objective function to reach the eventual optimum, it is not possible to employ very computationally expensive methods such as the finite element method (FEM) and computational fluid dynamics (CFD) used by aircraft OEMs for their final designs, as these take a long time on an extensive computational infrastructure to complete just one analysis. Instead, MDO often employs analyses which are simplified using assumptions based on knowledge of the system in question. However, since the Flying V concept is still in an early phase where such fundamental knowledge of the intricacies involved in its design are not well known, it is not always safe to assume such methods will work for this design.

Therefore, the data from previous research into the Flying V is used, augmented by methods based on first principles which are widely applicable. This results in an analysis which captures the essence of the complete aircraft design which is fairly accurate as long as the deviation from the designs used in the previous research is not too large.

Since for this study the topic of interest is the design concept, a single design is evaluated instead of a complete family such as has been done by Oosterom [22]. The variant chosen is the largest family member, the -1000, since in a product family design the largest member usually drives most sizings of common components. Therefore, it is expected that this variant will be closest to a version which is optimised as part of a family design.

Three configurations are modeled in this paper:

- **Conventional**: Tube-and-wing reference aircraft modeled to closely resemble the Airbus A350-1000. The inputs used for this model can be found in Appendix A.
- **Baseline**: Flying V configuration before optimisation, based on the Flying V-1000 resulting from the study by Oosterom [22]
- **Optimised**: Flying V configuration resulting from the optimisation in this study

[1] http://www.parapy.nl/

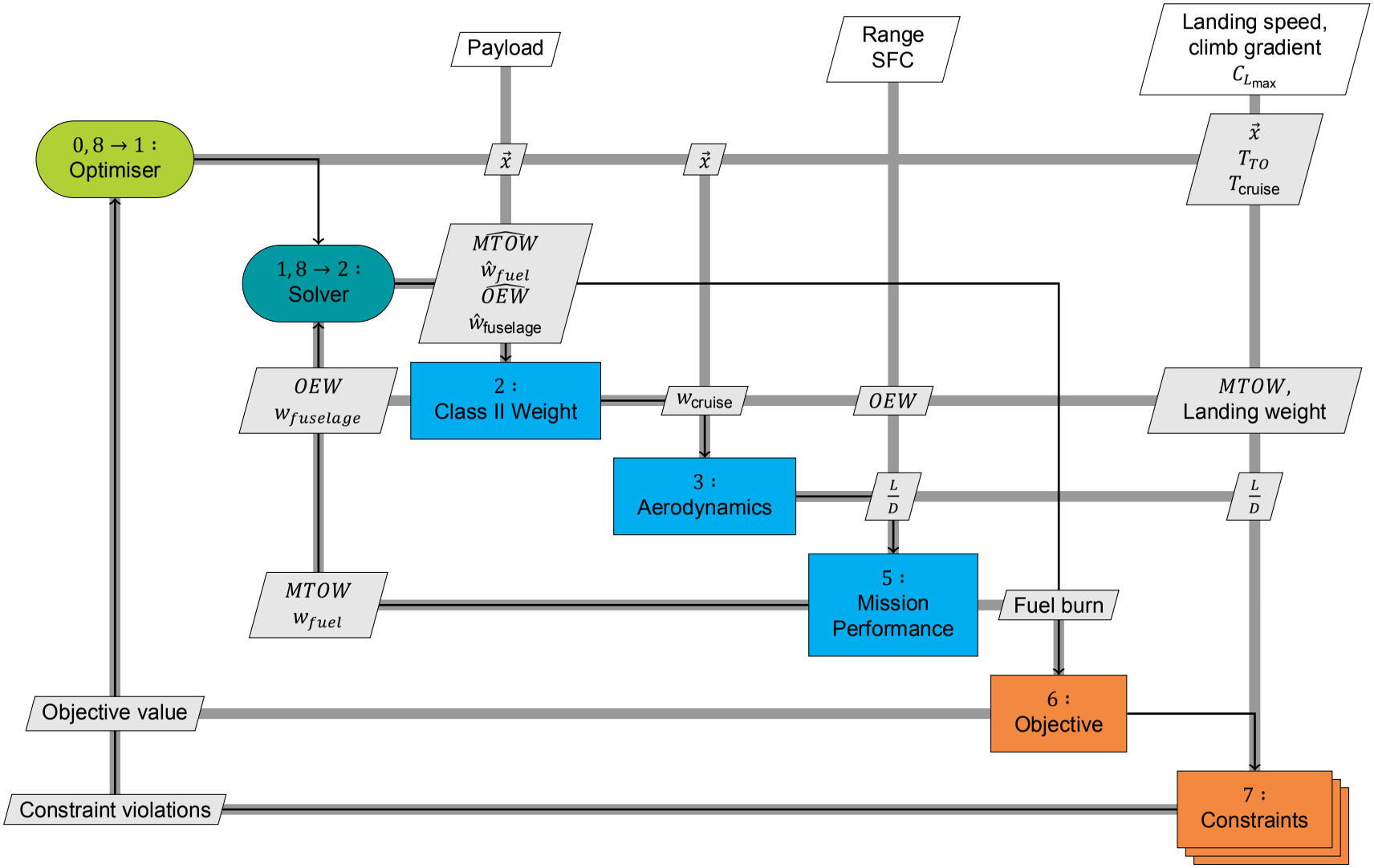

Figure 3.1: Extended design structure matrix of the research setup

3.1. Loading Diagrams

One of the driving requirements in many aircraft designs is the ultimate load factor, as many parts of the structure of the aircraft will be sized based on this number. The load factor is determined using loading diagrams, which visualise the load factor the aircraft is expected to experience in a number of predetermined situations, such as when experiencing a gust while flying at cruise speed. These situations are laid out in the relevant certification standards, which for aircraft such as the Flying V is the CS-25 standard [7].

Usually for large, long-range passenger aircraft the maximum load factors (both positive and negative) are determined by the minimum values established in CS-25, being $2.5g$ positive and $1.0g$ negative, as the gust loadings are usually well within these limits. For the Flying V, however, this may not be the case as the concept inherently has a much larger wing area than a comparable conventional aircraft. Therefore, the loading diagrams for the Flying V as well as the reference aircraft were constructed, see Figure 3.2.

It can be seen that, contrary to the expectation set by the larger wing area of the Flying V, the gust loading lines are even further within the minimum values than for the reference aircraft. This can, however, be easily explained by looking at the Flying V lift slope, C_{l_α}, which is much lower than it is for the reference aircraft. The Flying V has a lift slope of about $2.7\frac{1}{\text{rad}}$ as determined from windtunnel results by Viet and van Uitert [17, 28], while for a typical conventional aircraft with high aspect ratio wings we can expect a value closer to $5\frac{1}{\text{rad}}$ [33].

The result in Figure 3.2b shows that the maximum load factors of $2.5g$ and $-1g$ can be used in this stage of the design. However, for a more detailed stage of the design it must be noted that the gust loading of the Flying V may not satisfy the assumptions used for the conventional design method, as there may be appreciable delay between the time when a vertical gust hits the nose of the aircraft and when it reaches the outer wings. A conventional aircraft will experience little if any delay since its wings are relatively perpendicular to the airflow.

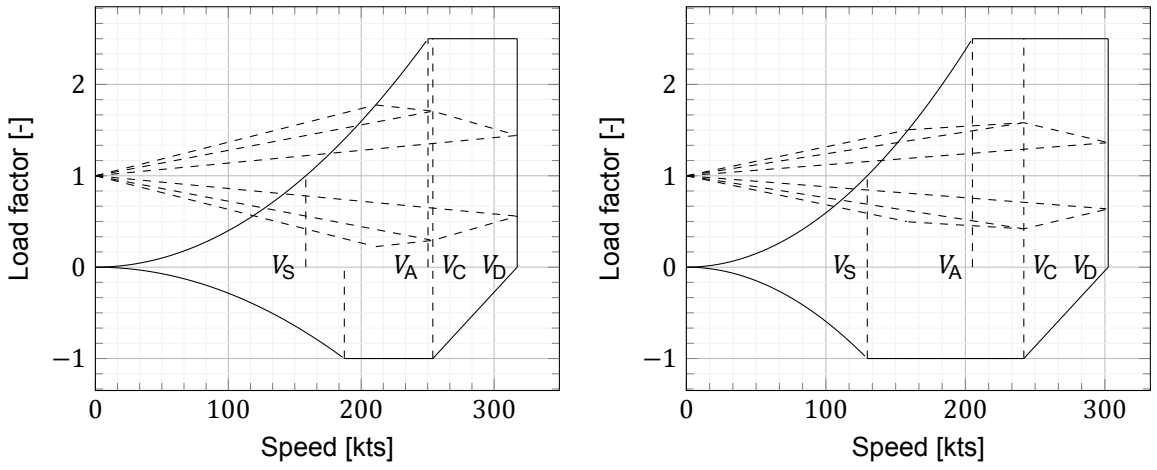

(a) Conventional aircraft

(b) Baseline Flying V

Figure 3.2: Loading diagrams

3.2. Weight Estimation

The weight estimation of the conventional aircraft follows the Class II weight estimation described by Torenbeek [32] with a few alterations to more closely match data published for the Airbus A350.

For the fuselage weight, the following equation is used:

$$w_{\text{fuselage}} = k_{\text{c}} k_{\text{pr}} k_{\text{wf}} \sqrt{V_{\text{D}} \frac{l_{\text{t}}}{b_{\text{f}} + h_{\text{f}}}} S_{\text{G}}^{1.2} \tag{3.1}$$

Where k_{c} is a correction factor of 1.1 added to match the data published for the Airbus A350, k_{pr} is a factor of 1.08 for pressurised fuselages, k_{wf} is a constant of proportionality, V_{D} is the dive speed, l_{t} is

the tail length, b_f and h_f are the fuselage width and height, respectively and S_G is the fuselage gross shell area.

For the furnishings weight, the following equation is used:

$$w_\mathrm{furnishings} = 0.196\mathrm{MZF}^{0.93} \tag{3.2}$$

Where the exponent was changed from 0.91 to 0.93 to match validation data presented by Basgall [34]

For all fixed equipment, the following equation is used:

$$w_\mathrm{fixed\ equipment} = k_\mathrm{fe}(w_\mathrm{surface\ controls}+w_\mathrm{APU}+w_\mathrm{instruments}+w_\mathrm{hydraulics}+w_\mathrm{electrics}+w_\mathrm{furnishings}+w_\mathrm{airco\ icing}+w_\mathrm{misc}) \tag{3.3}$$

Where k_fe is a correction factor of 1.1 added to match the model of the conventional aircraft to the weight of the Airbus A350.

For the engine weight approximation, a rubber engine sizing procedure was used, meaning that instead of choosing from a discrete set of available engines, the engine is allowed to ”stretch” with the design. This means that an estimation is necessary to obtain the engine weight of this stretched engine. Roskam’s part V [35] provides a set of data with a trendline for engine weight versus takeoff thrust, based on data from Jane’s All the World’s Aircraft, 1985 version [36]. For the engine weight estimation in this study, it is assumed that the slope of this relation on the logarithmic axes, i.e. the exponent of the equation, is also applicable to modern engines. The equation is then adjusted to correspond to state-of-the-art engines by making sure it passes through the data for the Rolls Royce Trent XWB-97 engine, 97000lbf of thrust at a weight of 16640lb. This results in the following equation:

$$w_\mathrm{engine} = \frac{T_\mathrm{TO}^{0.98}}{4.2} \tag{3.4}$$

For the wing weight prediction the method of Torenbeek’s Appendix C was used, as this method separately estimates the weight of the HLDs, allowing for a calculation without them which will be used below in the Flying V structure weight estimation. This detailed method is based on a root bending moment estimation, and as such requires the total wing weight as an input, as any weight in the wing will act as bending moment relief by countering lift. Since wing weight is both input and output, an iterative procedure is needed, visualised in Figure 3.3 for the case with HLDs included. The iteration loop for the case without HLDs is similar but omits the blocks for flaps and slats.

For the estimation of the weight of the Flying V, a combination of methods is used. For most weight groups it is safe to assume that their weight does not differ significantly from the weight of equivalent groups in the conventional aircraft. For these groups, the same method is used as for the conventional configuration.

A more challenging part of the weight estimation process for an unconventional configuration such as the Flying V is the structure weight estimation, since existing handbook methods such as the Torenbeek Class II method are not always valid. Therefore, results of previous studies into the Flying V are combined with conventional methods. An overview of this combination is shown in Figure 3.4.

The FEM analyses performed by Claeys [31] for both the Flying V and a conventional reference aircraft are combined with the structure weight estimation from the Torenbeek Class II weight estimation to obtain a baseline value of the total structure weight. It is assumed that the weight savings for the Flying V FEM weight as compared to the reference aircraft FEM weight are only reflected in the primary structure weight, not in the secondary structure weight. Therefore, the value obtained from the Class II weight estimation for the structure weight of the reference aircraft is split into primary and secondary structure using a value of 60% primary structure based on Droegkamp [37], see the following equation:

$$w'_\mathrm{st} = 0.60 w_\mathrm{st} \tag{3.5}$$

Where w'_st is the primary structure weight. The secondary structure weight logically follows as 40% of the total structure weight.

Since FEM weight is much smaller than actual primary structure weight a conversion factor is needed. This conversion factor is obtained by comparing the FEM weight for the reference aircraft with a Class II structure weight estimation performed for the same inputs as the FEM model, with the important difference that HLDs are not included since the Flying V does not feature any. The resulting

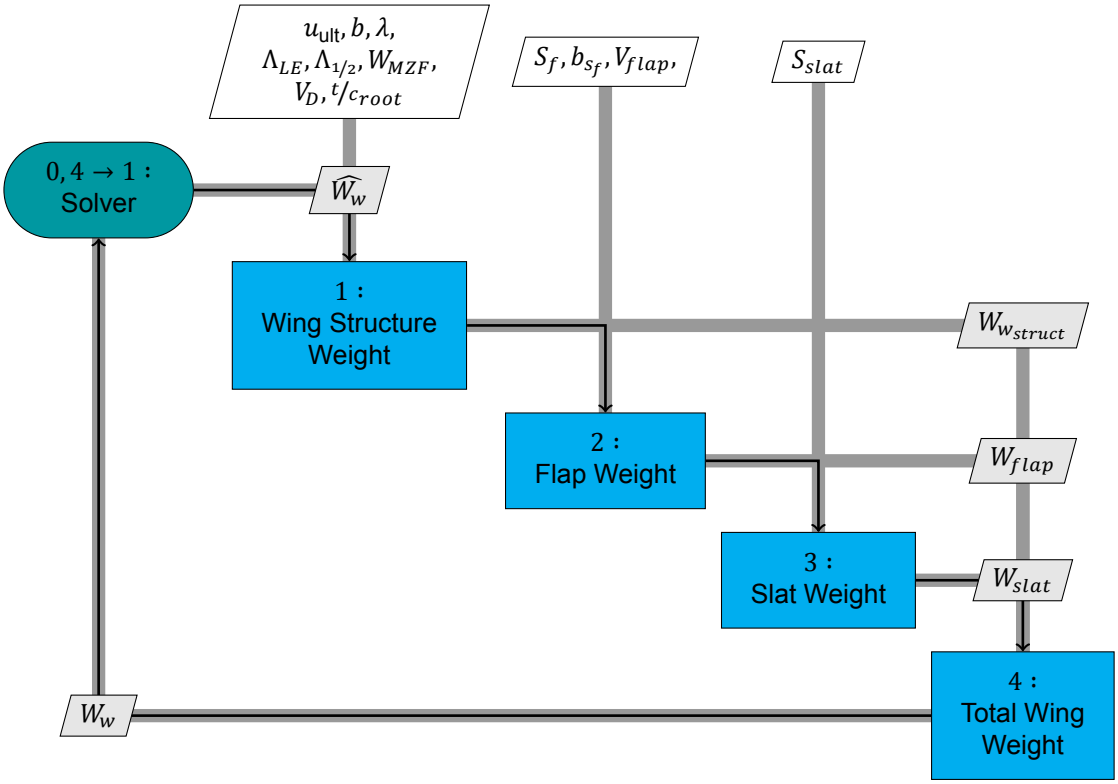

Figure 3.3: Wing weight iteration loop for the conventional aircraft

calculation is shown in the following equation:

$$\left(\frac{w'_{\text{st}}}{w_{\text{FEM}}}\right)_{\widehat{\text{FV}}} = \left(\frac{0.60 w_{\text{st}}}{w_{\text{FEM}}}\right)_{\widehat{\text{conv-HLDs}}} \tag{3.6}$$

Where the hat operator indicates that the configuration is the one used for the FEM analysis.

Combined with the Flying V FEM weight this gives the estimated primary structure weight. The secondary structure weight is assumed equal to that of the conventional aircraft since FEM analysis only considers supporting structures. Combining this gives the total structure weight for the Flying V configuration considered in the FEM analysis:

$$w_{\text{st}_{\widehat{\text{FV}}}} = w_{\text{FEM}_{\widehat{\text{FV}}}} \left(\frac{0.60 w_{\text{st}}}{w_{\text{FEM}}}\right)_{\widehat{\text{conv-HLDs}}} + 0.40 \left(w_{\text{st}}\right)_{\widehat{\text{conv-HLDs}}} \tag{3.7}$$

However, for the optimisation in this project, changes in both weight and geometry must be taken into account. For the changes in weight this is achieved by assuming the structure weight will scale with the maximum zero fuel weight (MZF), i.e. the structure will be a fixed percentage of the MZF:

$$w^{\star}_{\text{st}_{\widehat{\text{FV}}}} = \text{MZF}_{\text{FV}} \left(\frac{w_{\text{FEM}_{\widehat{\text{FV}}}} \left(\frac{0.60 w_{\text{st}}}{w_{\text{FEM}}}\right)_{\widehat{\text{conv-HLDs}}} + 0.40 \left(w_{\text{st}}\right)_{\widehat{\text{conv-HLDs}}}}{\text{MZF}_{\widehat{\text{FV}}}} \right) \tag{3.8}$$

Where the star indicates that the weight of this configuration differs from the weight used in the FEM analysis.

To account for the effect of changes in geometry on the structure weight, the fuselage weight estimation method developed for the Flying V by Oosterom [22] was used to adjust the percentage of MZF found above. This method requires a simplified loading as input, for which the weight groups presented in this section are used. The outer wing weight is estimated for this purpose with the same method as

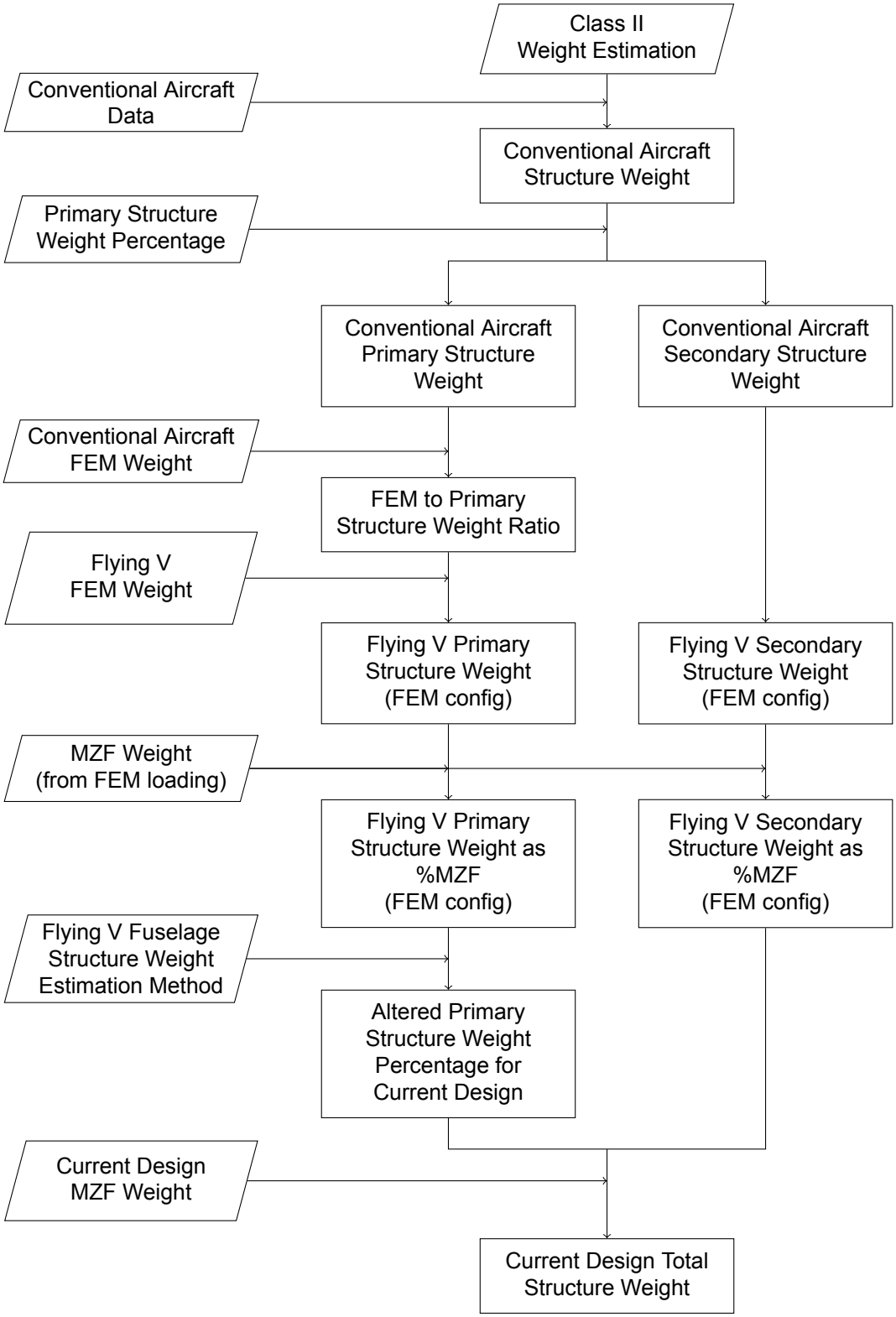

Figure 3.4: Structure weight estimation setup for the Flying V

the conventional configuration without HLDs. To get an estimate for the aerodynamic loads, the Athena Vortex Lattice (AVL) program by Drela [38] is run for the cruise condition.

This fuselage weight estimation method is executed for the currently evaluated design point. The value for fuselage and outer wing weight are then compared to a baseline value. The resulting ratio is used to adjust the primary structure weight percentage of MZF, see the following equation:

$$w_{\mathrm{st_{FV}}} = \mathrm{MZF_{FV}} \left(\frac{w_{\mathrm{fus}} + w_{\mathrm{w_{out}}}}{\hat{w}_{\mathrm{fus}} + \hat{w}_{\mathrm{w_{out}}}} \frac{w_{\mathrm{FEM_{\widehat{FV}}}} \left(\frac{0.60 w_{\mathrm{st}}}{w_{\mathrm{FEM}}} \right)_{\widehat{\text{conv-HLDs}}}}{\mathrm{MZF_{\widehat{FV}}}} + \frac{0.40 \left(w_{\mathrm{st}} \right)_{\widehat{\text{conv-HLDs}}}}{\mathrm{MZF_{\widehat{FV}}}} \right) \tag{3.9}$$

The inputs for this method are not known for the configuration used by Claeys however, so to obtain the baseline value the fuselage weight estimation method is executed for the known inputs of Claeys' configuration, after which the overall performance model is used to iteratively find a baseline value for which the structure percentage of MZF matches the value found above.

3.3. Aerodynamics

For the current study, the aerodynamic data needed are the cruise phase performance and the maximum lift coefficient (since the Flying V has no High-lift devices there is only one $C_{L_{\max}}$). The cruise performance is needed for the mission fuel burn analysis, while the maximum C_L is used for the stall speed, approach speed and climb gradient evaluations.

For the cruise performance, data from the thesis of Faggiano [27] are used, as they represent an aerodynamically optimised, full-scale aircraft. From this data, an approximated drag polar is constructed:

$$C_D = C_{D_0} + \frac{C_L^2}{\pi A e} \tag{3.10}$$

Where C_{D_0}, is the zero-lift drag coefficient, A is the aspect ratio and e is the Oswald efficiency factor. In order to account for changes in the geometry during the optimisation, this drag polar must be altered based on the design changes.

It is assumed that the Oswald efficiency factor remains unchanged, as it is expected that aerodynamic optimisation during further design can result in a span loading similar to that achieved by Faggiano. The zero-lift drag coefficient, C_{D_0}, is assumed to be dependent mostly on the wetted area, see the following equation:

$$C_{D_0} = \hat{C}_{D_0} \frac{S_{\mathrm{w}}/S_{\mathrm{ref}}}{\hat{S}_{\mathrm{w}}/\hat{S}_{\mathrm{ref}}} \tag{3.11}$$

Where S_w is wetted area, S is reference or planform area, and the values with a hat are the baseline values from Faggiano's thesis. The aspect ratio is simply calculated from the new geometry.

The method above would be sufficient for an aircraft operating in incompressible flow. However, the Flying V is designed to operate at a high-subsonic Mach number of 0.85, where compressibility effects are a significant part of the aerodynamic performance. To ensure designs are only chosen if they are not expected to suffer from excessive compressibility drag, the relation in the following equation from Torenbeek [39] is used:

$$M_{\mathrm{dd}} \cos \Lambda_{\mathrm{w}} + \frac{\left(\frac{t}{c} \right)_{\mathrm{w}}}{\cos \Lambda_{\mathrm{w}}} + 0.10 \left\{ \frac{1.1 \hat{C}_L}{(\cos \Lambda_{\mathrm{w}})^2} \right\}^{1.5} = M^{\star} \tag{3.12}$$

This equation relates the drag divergence Mach number, M_{dd}, to the mid-chord sweep, Λ_{w}, the average thickness-to-chord ratio, $\left(\frac{t}{c} \right)_{\mathrm{w}}$, and the wing lift coefficient, $\hat{C}_L$. The last value, $M^{\star}$, represents an airfoil technology factor which is constant for a given generation of airfoils.

For application to the Flying V design, this relation is applied for both the inner and the outer wing, separately, as a constraint to the optimisation. The value for M_{dd} is related to the required cruise speed from the mission specification, being 0.03 higher than the cruise Mach number. The value for $M^{\star}$ is found by applying Equation 3.12 to the design resulting from Faggiano's work, as this gives an approximation of the technology factor which can be expected of the inner and outer wing airfoils. The

resulting values of M^* are 0.91 for the inner wing and 0.93 for the outer wing, which is close to the value stated by Torenbeek of 0.935.

For the reference aircraft evaluation, a drag polar similar to that of the Flying V is constructed. Since no input data is available for the zero-lift drag, C_{D_0}, this has to be estimated using analytical methods. The method used is a combination of flat-plate skin friction coefficient, C_f, based on the von Kármán-Schoenherr curve found in Obert [40] with form factors which capture the contribution of pressure drag. The relations for the form factor of lifting bodies and bodies of rotation are found in Hoerner [41]. For the fuselage form factor, figure 40-20 from Obert [40] is used instead. The nacelle form factor relation was changed after validation to use the method proposed by Raymer [42], see section 4.2

3.4. Engine Inputs

The fuel burn model and constraint calculations used in the optimisation require only basic information about the engines; specific fuel consumption (SFC), maximum takeoff and continuous thrust and the engine weight. The specific fuel consumption is 15 g/kN/s, slightly higher than the cruise fuel consumption of the Rolls Royce Trent XWB engines used on the Airbus A350[2] to account for off-design conditions performance. Although it can be expected that a newer generation engines with lower fuel consumption will be available for the Flying V, the values for the Trent XWB are more certain and provide a better comparison of the Flying V concept with the tube-and-wing concept using current aircraft for comparison. The takeoff thrust is set as a design variable, since the required thrust is dependent on the aerodynamic performance and weight of the configuration being calculated. The maximum continuous thrust is taken as a fixed percentage of 90% of the takeoff thrust, in accordance with the Trent XWB data.

In reality, both thrust and fuel burn characteristics of engines change with altitude and Mach number. For simplicity, in this study these differences are not included and constant values are used.

3.5. Mission Performance Analysis

The analyses described above are combined into a mission performance analysis. For the calculation of the mission fuel burn, the fuel fractions method as described by Roskam [43] is applied to the mission profile shown in Figure 3.5.

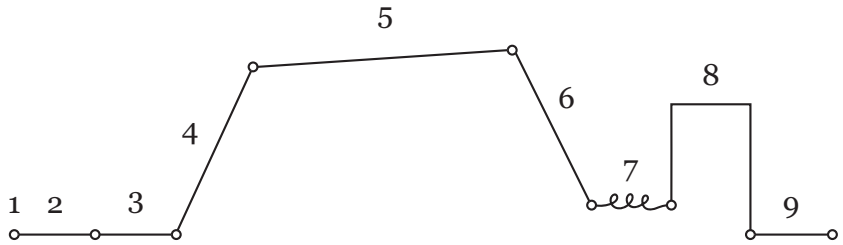

1. start & warm-up	4. climb	7. loiter
2. taxi	5. cruise	8. diversion
3. take-off	6. descent	9. landing, taxi, shut-down

Figure 3.5: Mission profile

For the cruise, diversion and loiter phases the Breguet range and endurance equations are used to determine the fuel fraction, while for the other segments Roskam lists fixed fuel fractions based on empirical data. For simplicity, it is assumed that the cruise strategy used is a continually climbing cruise, which ensures that the aircraft flies at its maximum L/D at all times. This can result in altitudes during cruise which exceed the service ceiling of the aircraft, which means the cruise performance in this model will be slightly better than in reality. For the Flying V model in this study the service ceiling refers to the altitude at which the design maximum pressure differential between the cabin and the outside air is reached, meaning that above this altitude proper cabin pressurisation cannot be achieved. Additionally,

[2] https://en.wikipedia.org/wiki/Rolls-Royce_Trent_XWB (visited on 20-8-2021)

the engine performance does not take the difference in altitude into account, rather simply relies on the inputs described in section 3.4.

For the shorter segments, the fixed fuel fractions listed by Roskam are not representative for a very long range mission such as the design mission of this study, since relatively much more fuel is used during cruise, which means the shorter segments which do not change with range must have lower fuel fraction values. Therefore, the climb fuel fraction is calculated using the Breguet endurance equation and the other fixed fuel fractions are adjusted with the same percentage with regards to the values listed by Roskam.

To calculate this climb fuel fraction, the Breguet endurance equation is used. However, for this equation the time to climb must be known. To obtain this time, the weight at the top of the climb, w_{toc} is calculated first. Assuming the weight at the end of the mission, w_9, is equal to the OEW plus the payload weight and reserve fuel, the segment weights can be calculated backwards through the mission:

$$w_{\text{toc}} = \frac{w_9}{\prod_{i=9}^{i=5} \left(\frac{w_i}{w_{i-1}} \right)} \tag{3.13}$$

This weight can be used to calculate the altitude for the top of climb, h_{toc}, as it is assumed that the entire cruise segment is flown at the maximum $\frac{L}{D}$, giving a constant C_L. The climb is flown at the maximum steady rate of climb, i.e. the C_L at which $\frac{{C_L}^2}{{C_D}^3}$ is maximum is chosen. Since this means flying an accelerated climb, the altitude is discretised into n segments, for each of which the rate of climb is calculated using the following equation:

$$\text{RC}_i = \frac{TV_i - D_i V_i}{w_i} \tag{3.14}$$

Where T is the maximum continuous thrust, D is the drag calculated for this segment's altitude and airspeed, and V is this segment's airspeed. Using this rate of climb, the time used and the horizontal distance covered for this segment can be calculated. These are then summed to obtain the time to climb, t_{climb} and the climb segment range credit, d_{climb}:

$$t_{\text{climb}} = \sum_{i=0}^{n} \frac{\frac{h_{\text{toc}}}{n}}{\text{RC}_i} \tag{3.15}$$

$$d_{\text{climb}} = \sum_{i=0}^{n} t_i \sqrt{V_i^2 - \text{RC}_i^2} \tag{3.16}$$

Where t_i is the time used for segment i. The fuel fraction is then calculated using Breguet's endurance equation. The resulting fuel fraction for climb is compared to the listed fuel fraction in Roskam of 0.97. This reduction is then also applied to the other fixed fuel fractions, resulting in the values in Table 3.1.

Table 3.1: Adjusted fuel fractions used for the mission performance analysis

Segment	Fraction
Warmup	0.9965
Taxi	0.9965
Takeoff	0.9983
Climb	0.9899
Descent	0.9965
Landing	0.9972

3.6. Optimisation

The analyses described above result in a complete model of the aircraft which can be optimised for a certain objective. This section discusses the setup of the optimisation, including the requirements which are input to the aircraft model, the design variables and the constraints.

The optimisation algorithm used is the differential evolution algorithm [44] as implemented in the Python package SciPy [45]. This is a genetic algorithm which is capable of working with irregular and non-differentiable cost functions, as well as being able to utilise parallel computing efficiently. These aspects make it a suitable choice for this study.

Table 3.2: Design variables with their bounds

Design variable	Symbol	Lower bound	Upper bound
Takeoff thrust	T_{TO}	360kN	500kN
Inner wing sweep	Λ_{n}	60°	70°
Outer wing sweep	Λ_{out}	30°	45°
Outer span (as % of total)	b_{out}	25%	50%
Length 1 (as % inner wing)	L_1	60%	85%
Chord 1 (as fraction of oval width)	c_1	1.08	1.5
Taper ratio	λ	0.05	0.3
Cabin width 1	w_1	5m	8m
Cabin width 3 (as % of w_1)	w_3	60%	100%
Crown height 1	H_{c_1}	0.5m	0.8m
Keel height 1	H_{k_1}	0.3m	0.6m
Crown height 3	H_{c_3}	0.5m	0.8m
Keel height 3	H_{k_3}	0.3m	0.6m
Outer wing thickness to chord ratio	$\frac{t}{c}_{\text{out}}$	7.5%	11.5%

The choice of the design variables is an important part of setting up a design optimisation system as every design variable adds a dimension to the design space and therefore increases the computational time needed for the optimisation. However, sufficient design variables must be chosen to ensure the optimiser has the freedom to find new design optimums. Additionally, defining the design variables well can prevent infeasible designs such as impossible geometries to be considered by the optimiser.

With these considerations in mind, the chosen design variables are presented in Table 3.2 along with the bounds set on them for the optimiser. A visualisation of the variables is shown in Figure 3.6.

For the objective function, the total mission fuel burn is chosen. Although there are other metrics to consider if the goal is to minimise global warming impact, as investigated by Proesmans [46], this is outside the scope of the current study. The fuel burn is considered an adequate metric as many of the impacts correlate roughly to the fuel burn, especially for a given engine. Additionally, the fuel burn represents the total energy used for the flight, which can become a more important characteristic when alternative energy sources are considered in the future, such as hydrogen. The optimisation can be mathematically described as follows:

$$\begin{aligned} \min_{\vec{x}\in\mathbb{R}^n} \quad & w_{\text{fuel}}(\vec{x}) \\ s.t \quad & \vec{g}(\vec{x}) \leq \vec{0} \end{aligned} \tag{3.17}$$

To initialise the aircraft model, certain aircraft requirements must be supplied which define what the aircraft is designed to accomplish. The main requirements are presented in Table 3.3, these requirements are based on Oosterom [22] to ensure a fair comparison between the baseline and optimised configurations.

Table 3.3: Requirements for the Flying V model

Requirement	Value	Unit
Passengers	378	[-]
Of which business	52	[-]
Cruise Mach	0.85	[-]
Design range	15750	[km]
Design payload	32	[10^3 kg]

The design range and payload were based on the payload-range diagram of the reference aircraft, A350-1000 [47]. The point on the diagram is chosen to be the maximum range where the total weight

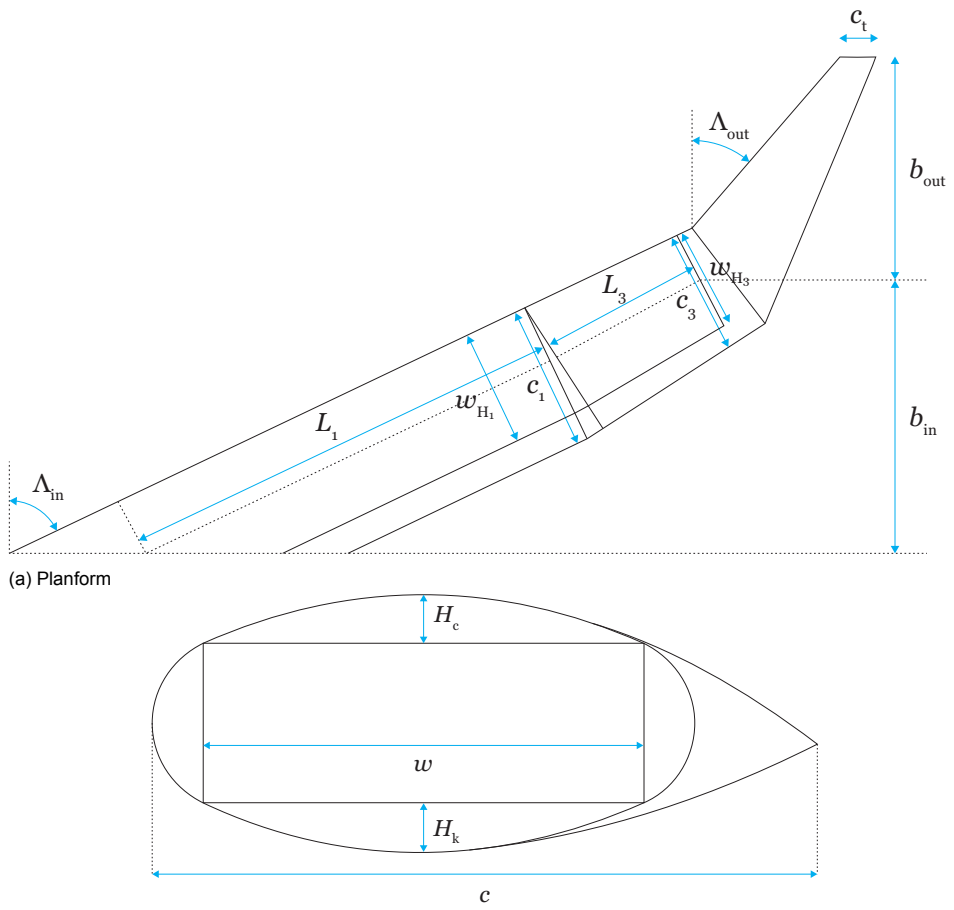

(a) Planform

(b) Cross section

Figure 3.6: Design Variables

is equal to the maximum takeoff weight (MTOW), meaning the fuel tanks are full. This point is deemed the most relevant since it is completely defined by aircraft performance and fuel tank size, as well as being the point close to which most missions are flown.

In addition to the requirements above, constraints which relate to operational requirements are needed to ensure the optimisation results in a feasible design. First, four performance constraints are defined, which are shown with their requirement values in Table 3.4.

Table 3.4: Performance constraints

Constraint	Value	Units
Approach speed	147	[kts]
Takeoff distance	3000	[m]
Cruise Mach	0.85	[-]
Climb gradient (OEI)	2.4	[%]

The Flying V has only one stall speed, due to the lack of HLDs, therefore there is only one requirement on the stall speed, which is set by the approach speed, V_{app} as it is the slowest airborne phase of a flight. The requirement for the approach speed is set at 147kts, since this is the approach speed of the reference aircraft, the Airbus A350-1000. The stall speed requirement is set lower, since flying an approach exactly at stall speed is unadvisable. The regulations in CS-25.125 [7] specify that the approach speed must be at least 23% higher than the stall speed, which means the stall speed requirement is 120 kts. The maximum lift coefficient, $C_{L_{max}}$ used in this calculation is 0.95, which is the maximum useable lift coefficient of the Flying V before an unstable pitch break occurs [28]. The

resulting constraint function is shown in the following equation:

$$g_1(\vec{x}) = \sqrt{\frac{w_{\text{landing}}}{C_{L_{\max}} \frac{1}{2}\rho S}} - 120 \qquad \text{[kts]} \tag{3.18}$$

The takeoff requirement is defined in terms of the takeoff parameter (TOP) presented in the following equation:

$$\text{TOP} = \frac{W}{S}\frac{W}{T}\frac{1}{\sigma}\frac{1}{C_{L_{\text{TO}}}} \tag{3.19}$$

Where $C_{L_{\text{TO}}}$ is the takeoff lift coefficient, defined as $C_{L_{\text{TO}}} = \frac{C_{L_{\max}}}{1.1^2}$ and σ is a correction factor for takeoff at altitude, which is zero since the requirement used is based on the reference aircraft's takeoff distance at sea level. The TOP is related to the takeoff distance by a graph in Raymer [42]. However, applying Equation 3.19 to known data of the A350-1000 results in a significantly higher TOP than would be expected using this graph. Therefore, the value calculated for the conventional aircraft is used as the requirement, resulting in the following constraint function:

$$g_2(\vec{x}) = \frac{W}{S}\frac{W}{T}\frac{1}{C_{L_{\text{TO}}}} - 140 \qquad \left[\frac{\text{kg}^2}{\text{m}^2 N}\right] \tag{3.20}$$

The requirement for cruise speed limits the continuous thrust produced by the engines to be at least sufficient to overcome the drag for the cruise Mach number at the top of climb, as this is the highest drag encountered during cruise. Therefore the requirement is simply equal to the cruise Mach number above. The constraint function is shown below.

$$g_3(\vec{x}) = D_{\text{toc}} - T_{\text{cont}} \qquad \text{[N]} \tag{3.21}$$

Where D_{toc} is the drag at the top of climb and T_{cont} is the maximum continuous thrust of both engines.

The climb gradient requirement is specified by CS-25.121 [7] at 2.4% for the one engine inoperative situation. To approximate this scenario, this calculation is performed with the (takeoff) thrust of one engine. However, additional drag due to the inoperative engine and any trim required to counteract the yawing moment induced by this asymmetric situation is neglected. This leads to the following constraint function:

$$g_4(\vec{x}) = 0.024 - \frac{\frac{1}{2}T_{\text{cont}}}{\text{MTOW}} - \left(\frac{C_D}{C_L}\right)_{\min} \tag{3.22}$$

In addition to the performance requirements, several geometrical constraints must be met for the aircraft to fulfil its mission, listed in Table 3.5.

Table 3.5: Geometry constraints

Constraint	Value	Units
Passenger cabin area	309	[m^2]
Cargo bay volume	250	[m^3]
Fuel tanks volume	Determined by fuel burn	[m^3]

The passenger area constraint calculates a minimum area needed in the passenger cabin to fit sufficient seats for all passengers, as well as aisles, galleys and toilets. This area is calculated using the method developed by Oosterom [22] and used to position the rear end of the passenger cabin in the ParaPy model. If the ceiling height at this end is at least 1.9m, the requirement is met. This is only relevant if the cabin extends into the tapered part of the oval fuselage, as the ceiling height in the untapered part is set at 2.25m.

The cargo volume constraint considers the part of the cabin aft of the area needed by the passengers. Based on the cargo volume of the reference aircraft, and using an assumed 80% usable space of the total volume, a value of $250m^3$ is set as the minimum volume of this compartment, as calculated by ParaPy.

The fuel is located in the aft part of the inner wing, behind the passenger cabin and cargo compartment, as well as in the outer wing between the front and rear spar. The volume of these locations can be calculated using the geometrical capabilities of ParaPy and related to the calculated total mission fuel burn to ensure there is sufficient space for the fuel.

A visualisation of the three geometry constraints is shown in Figure 3.7. Note that the interruption of the inboard fuel tanks caused by the engine and landing gear structure is moved to the centreline for ease of calculation, as this part is not tapered the volume does not change by this shift.

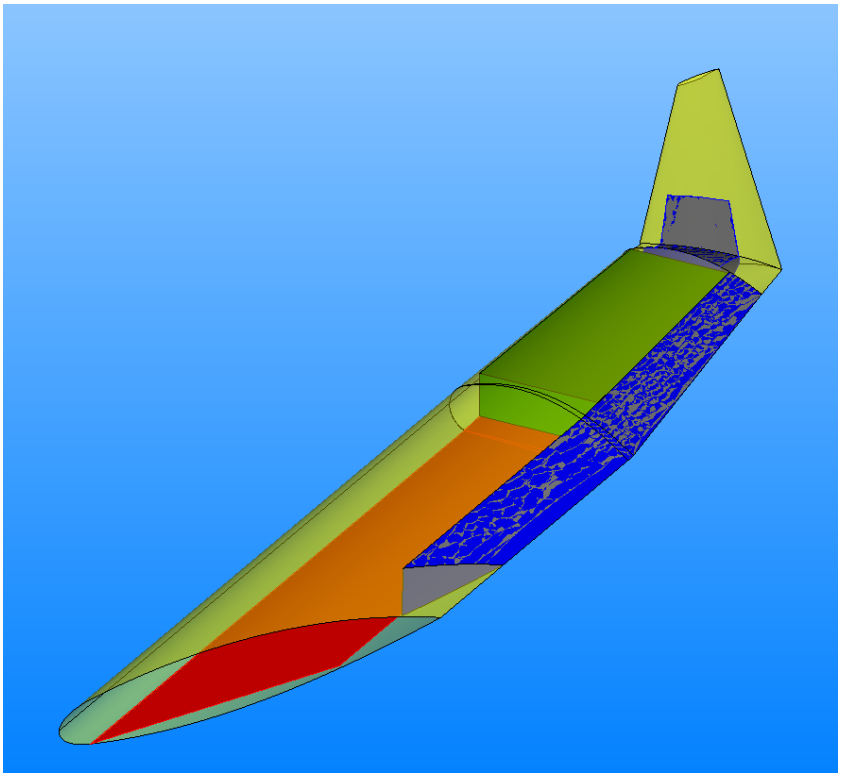

Figure 3.7: Geometry constraint shapes as defined in ParaPy, cabin floor in red, cargo volume in green and fuel tanks in blue

Finally, the compressibility correction discussed in section 3.3 is also added as a constraint to the optimisation:

$$g_8(\vec{x}) = M_{\text{dd}} \cos\Lambda_{\text{w}} + \frac{\left(\frac{t}{c}\right)_{\text{w}}}{\cos\Lambda_{\text{w}}} + 0.10\left\{\frac{1.1\hat{C}_L}{(\cos\Lambda_{\text{w}})^2}\right\}^{1.5} - \hat{M}^{\star} \tag{3.23}$$

Where $\hat{M}^{\star}$ is 0.91 for the inner wing and 0.93 for the outer wing, as discussed in section 3.3.

4

Verification & Validation

This chapter describes the process of verifying and validating the developed performance model. Section 4.1 discusses the weight estimation method, section 4.2 is concerned with the aerodynamic model, section 4.3 looks at the entire mission performance analysis and in section 4.4 a sensitivity analysis is performed.

4.1. Class II Weight Estimation

For the validation of the Class II weight estimation, data from Roskam [35] is used, as well as data from a comparative study of weight estimation methods by Basgall, Lui, Cassady and Anemaat [34]. Roskam provides data for most weight groups used in the estimation, based on a variety of reference aircraft. This allows for the comparison of individual weight groups against this reference data. In this section, several weight groups of interest are highlighted: groups for which the relations were edited and higher-level weight groups which give an indication of the validation of the weight groups of which they are composed.

Two weight groups for which the relations were edited with respect to the original method are the fuselage and the furnishings, these are shown related to the reference data in Figure 4.1a and Figure 4.1b. The data for the fuselage in this graph shows good correspondence with the reference data. As can be seen in the graph, the furnishings weight is lower than the reference data, but is deemed acceptable since the method matches the data presented by Basgall et al. [34]. Furthermore, the total fixed equipment weight shown in Figure 4.1e includes the furnishings weight, and it shows a good correspondence with the reference data.

The empennage weight is slightly lower than expected for an aircraft of this weight, with a weight of 4.2t for both variants since the tail surface configuration is identical between them. However, as shown in Figure 4.1c, it matches the reference data well when compared to the total empennage area. This indicates that the Airbus A350 has a relatively small empennage, and that the method does not need any adjustments.

Since the more extensive estimation method from Torenbeek's appendix C [32] was used, the wing weight estimation is examined closely as well. The result is shown in Figure 4.1d, showing a good match with the reference data.

The end result of the weight estimation, the total empty weight of the conventional aircraft model, shows good correspondence with the reference data, see Figure 4.1f. This empty weight value can also be compared to the empty weight of both Airbus A350 variants for a more specific validation. The empty weight for the A350s is derived from their payload-range diagrams, see Figure 4.2. The empty weight of an aircraft can be deduced from the payload-range diagram when the fuel tank volume is known, as this gives the total fuel weight when tanks are full; i.e. at the design point indicated in the graph. When the maximum fuel weight and the payload at this point are subtracted from the MTOW, this gives the operational empty weight (OEW).

The correspondence between the model and the published data is very good, with an OEW of 142t for the A359 versus 144t for the corresponding model, and 157t for the A351 versus 156t for its corresponding model.

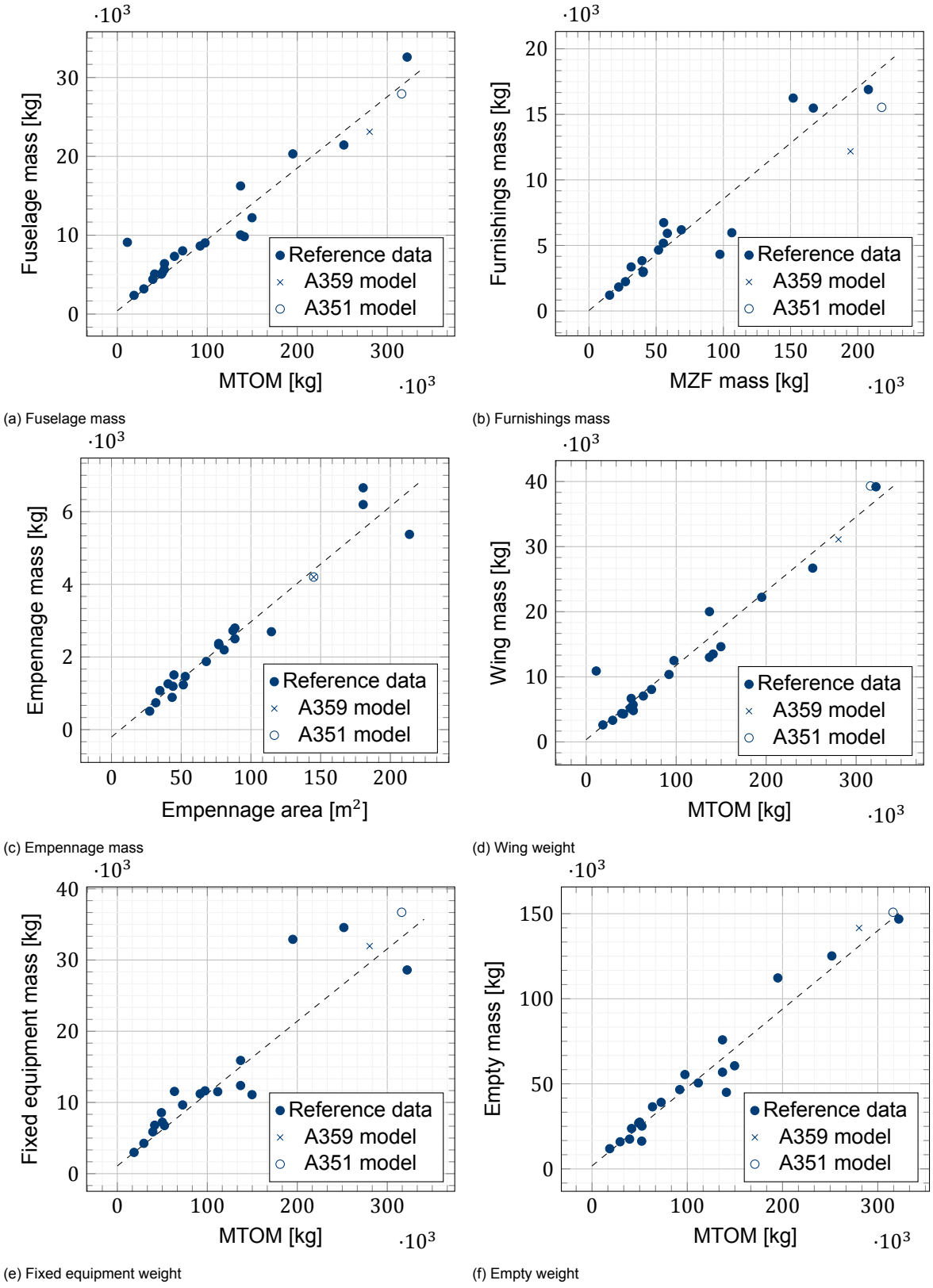

(a) Fuselage mass

(b) Furnishings mass

(c) Empennage mass

(d) Wing weight

(e) Fixed equipment weight

(f) Empty weight

Figure 4.1: Validation data for the major weight groups of the conventional aircraft model, both variants

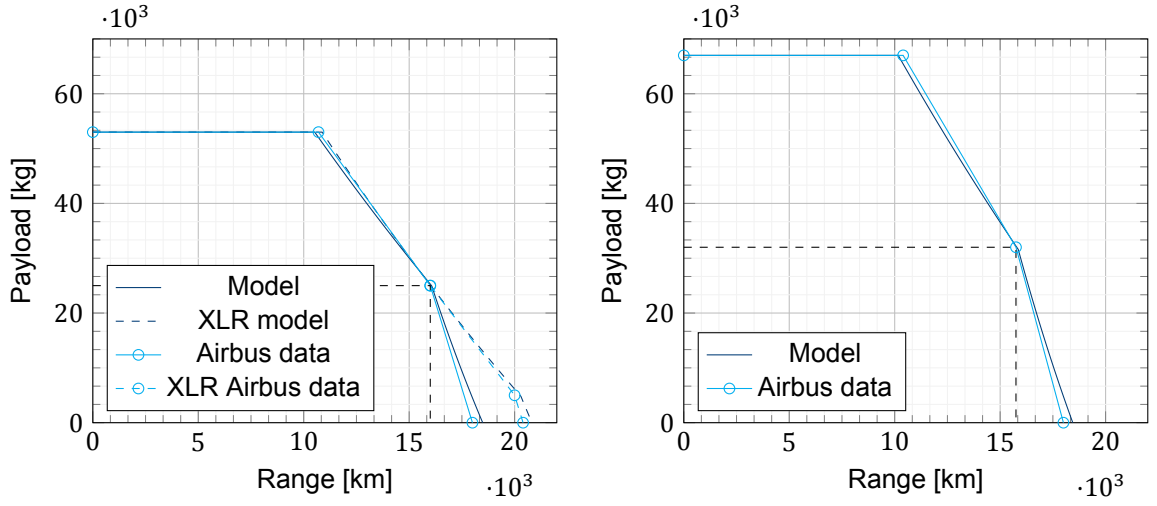

(a) A359, XLR indicates the extra long range version

(b) A351

Figure 4.2: Payload-range diagram for the conventional aircraft model compared to the data for the Airbus A350

4.2. Aerodynamic Model

For the aerodynamic analysis, two main points are important in the validation: the zero-lift drag and the Oswald factor.

For the zero-lift drag, C_{D_0}, the data modeled for the conventional aircraft are compared to a wind-tunnel test performed on the NASA Common Research Model (CRM) [29, 48]. This data is shown in Table 4.1. The test run used was performed at a Mach number of 0.85 and a Reynolds number of 30 million, which are representative flight conditions for this aircraft. However, the wind tunnel model did not have a vertical tail or nacelles for this run. Therefore, the C_{D_0} of the modeled aircraft without these contributions is compared to the wind tunnel data. With a value of 123 drag counts for the wind tunnel test against 119 drag counts for the model, the zero-lift drag is deemed validated.

Table 4.1: Aerodynamic model validation data for aircraft without vertical tail and engines

Metric	NASA CRM	A351 model	A359 model
C_{D_0}	123	119	126
e	0.753	0.75	0.73

The Oswald factor is also compared to the NASA CRM. At the lift coefficient flown for $\frac{L}{D}\max$ it was calculated to have an Oswald factor of 0.753, very close to the 0.75 found for the A359 model. This was deemed satisfactory validation for the aerodynamic model, also for the Oswald factor of 0.73 found for the A351 due to its larger fuselage.

4.3. Mission Analysis

The entire mission analysis can be validated using the payload-range diagrams for the A350, shown in Figure 4.2. The slopes of the payload-range diagram are an indication of overall efficiency of the aircraft, a combination of aerodynamics, weight and engine efficiency. With the aerodynamics and weight validated, a good match in slope between the model and the data published by Airbus [47] indicates a mission performance analysis model which is close to reality. As the slopes in these graphs are very close to the published data, the mission analysis method is deemed validated.

4.4. Sensitivity Analysis

In this section, the impact of important assumptions made in the development of the performance model on the fuel burn of the Flying V is investigated. Firstly, since the aerodynamic loading input of the inner wing structure weight calculation is based on a single situation evaluated with AVL, the centre of gravity

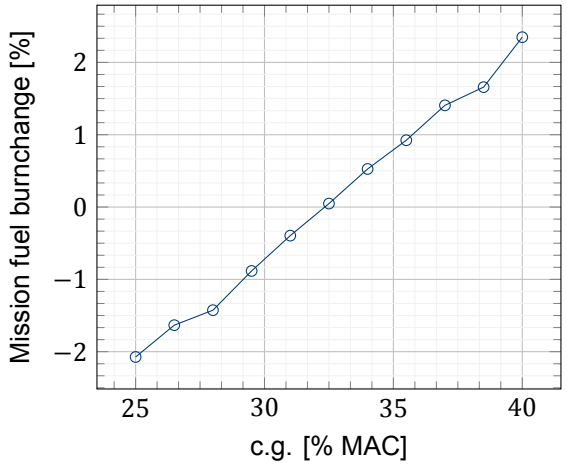

(a) Centre of gravity location as a percentage of the MAC

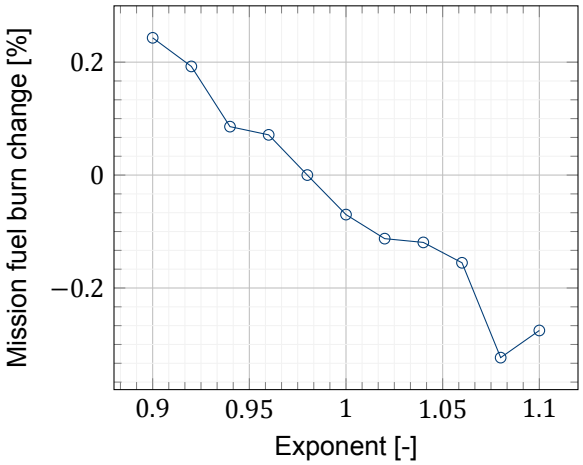

(b) Engine weight estimation

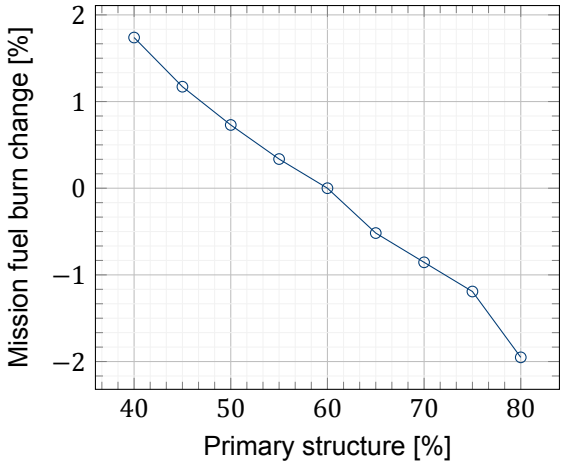

(c) Primary structure weight percentage

Figure 4.3: Sensitivity analysis data of three assumptions

in this situation has an impact on the loading and thus on the structure weight. A range of locations of the centre of gravity from 25% to 40% of the mean aerodynamic chord is evaluated for the model of the Flying V to obtain the mission fuel burn, the result is shown in Figure 4.3a. The result shows that a more forward centre of gravity yields a lower fuel burn. This is to be expected since a forward shift in weight distribution results in a forward shift in lift distribution for equilibrium, which for the Flying V also means a shift inboard resulting in lower bending loads. The impact on aerodynamic efficiency of this change in lift distribution is not taken into account. Since the total change in fuel burn is limited to about 2%, the impact of the centre of gravity is not deemed a problem for the validity of the model.

The second assumption for which the sensitivity is analysed is the rubber engine weight estimation described by Equation 3.4 in section 3.2. Since the exponent of this equation was derived from a figure, it should be checked for impact on the overall model. To do this, the exponent is changed from 0.9 to 1.1. However, before application the equation is still tuned to match the Rolls Royce Trent XWB data so that it represents modern engines. As can be seen from Figure 4.3b, the impact of this exponent on the fuel burn is very minor. This is to be expected since the bounds on the takeoff thrust in the optimisation are close to the value for the Trent XWB engine for which this formula is tuned.

Finally, the assumption that 60% of the structure weight of the conventional aircraft is comprised of primary structure and 40% of secondary structure is evaluated. This fraction is based on a study by Droegkamp [37], who states that the actual primary weight percentage may vary from 40% to 80%. Therefore, this range of percentages is input into the model, resulting in Figure 4.3c. This figure shows a decrease in fuel burn with an increase in primary structure percentage, which is logical since the decrease in FEM weight described by Claeys [31] was only applied to this primary structure and not to

the secondary structure. The minor impact of under 2% of the total fuel burn shows that this assumption does not considerably impact the validity of the model.

5

Results and Discussion

This section discusses the results of the analysis of the baseline Flying V, as well as the analysis of the design resulting from the design optimisation. Section 5.1 presents the results of the baseline design and section 5.2 gives discusses the geometry and performance results of the optimised configuration.

5.1. Baseline Design

The performance analysis model described in chapter 3 is applied to the baseline aircraft, which is the -1000 variant of the Flying V design as presented by Oosterom [22]. Important metrics resulting from this calculation are presented in Table 5.1, the payload-range diagram is presented in Figure 5.1.

In comparison to the analysis performed for this baseline design in the original study by Oosterom [22], the current analysis model shows markedly improved performance in mission performance. Although the OEW is unchanged, the total fuel burn is 16% lower thanks to the higher lift-to-drag ratio used in the current model. The aerodynamic analysis performed by Oosterom employs the vortex lattice method AVL with the parameterised geometry as input, combined with a viscous module since AVL uses non-viscous calculations. This geometry-based approach is very suitable for the comparison between family members as performed by Oosterom. However, the geometry is based on the geometry parameterisation by Hillen [49], which was identified by Hillen to be less aerodynamically efficient than the optimised geometry by Faggiano [27], and no in-depth aerodynamic optimisation was performed to mitigate this. Therefore, the method used in the current study, based on the optimised results by Faggiano, is deemed to better represent the potential of the concept of the Flying V since it can be expected that aerodynamic optimisation such as performed by Faggiano will be part of the further development of the aircraft.

Compared to the conventional reference aircraft, a fuel burn saving of 31% is achieved, with a 21% reduction in MTOW. The payload range efficiency (PRE), shown in Table 5.1 shows a similar trend, since the design missions of all configurations are nearly equal. Payload range efficiency is defined by the following formula [50]:

$$\text{PRE} = \frac{w_{\text{pl}} \cdot R}{w_{\text{fuel}}} \tag{5.1}$$

The payload-range diagrams show differences in harmonic range and ferry range. The aerodynamic efficiency of the Flying V concept is higher than that of a conventional aircraft, a consequence of this is that the slope of the payload-range diagram will decrease, since less fuel is needed for a given increase in range and therefore less payload needs to be removed. For the given design point this means that the harmonic range will be decreased and the ferry range increased.

5.2. Optimisation Results

This section presents the results for the optimised configuration, starting with the resulting geometry, followed by the mission performance results and a discussion regarding constraint compliance.

[1] Personal communication with R. Vos, value obtained using method from Oosterom [22]

Table 5.1: Performance metrics for the conventional, baseline and optimised configurations. Original data for the baseline design are found by Oosterom [22].

Metric	A351 model	Baseline		Optimised	Unit
		Original data	Modeled		
MTOW	315	266	248	237	[10^3 kg]
OEW	156	129	129	122	[10^3 kg]
Fuel (design mission)	127	103	87	82	[10^3 kg]
Payload Range Efficiency	3.97	5.08	5.79	6.15	[10^3 km]
Structure weight		60	56	50	[10^3 kg]
$\frac{L}{D}_{\max}$	19.3	20.6	23.5	23.9	[-]
C_{D_0}	147	54[1]	56	56	[drag counts]
Oswald factor	0.73	0.81[1]	0.86	0.86	[-]
S_{ref}	439	921	921	885	[m^2]
$\frac{T}{W}$	0.279	0.285	0.305	0.322	[-]
$\frac{W}{S}$	718	289	269	268	$\left[\frac{\text{kg}}{\text{m}^2}\right]$

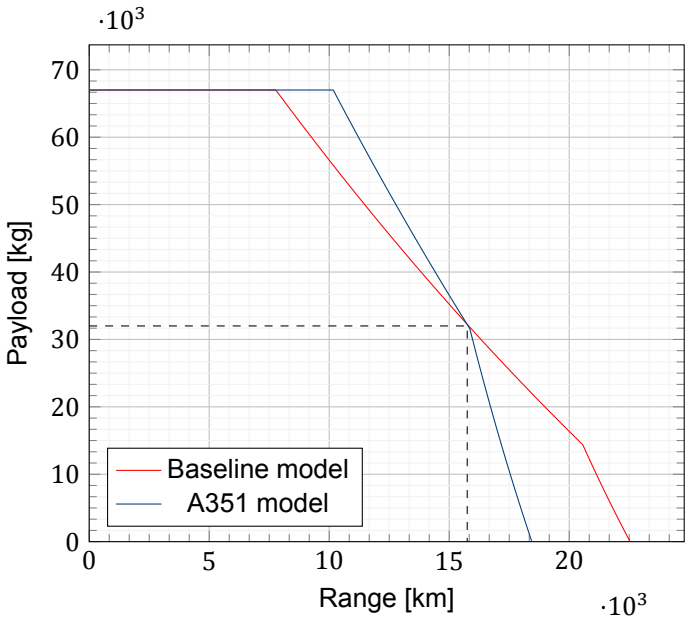

Figure 5.1: Payload-range diagram for the baseline Flying V

5.2.1. Optimised Geometry

The optimised design planform is shown in Figure 5.2 superimposed on the baseline design planform. A visualisation of the cabin cross-sections is given in Figure 5.3. The design variables for the baseline and optimised designs are shown in Table 5.2.

Table 5.2: Design variables for the baseline and optimised configurations

Design variable	Symbol	Baseline	Optimised
Takeoff thrust	T_{TO}	371kN	374kN
Inner wing sweep	Λ_n	64.5°	63.2°
Outer wing sweep	Λ_{out}	40.7°	41.1°
Outer span (as % of total)	b_{out}	34%	29%
Length 1 (as % inner wing)	L_1	75%	67%
Chord 1 (as fraction of oval width)	c_1	1.11	1.3
Taper ratio	λ	0.1	0.11
Cabin width 1	w_1	6.2m	5.94m
Cabin width 3 (as % of w_1)	w_3	94%	82%
Crown height 1	H_{c_1}	0.68m	0.63m
Keel height 1	H_{k_1}	0.68m	0.50m
Crown height 3	H_{c_3}	0.45m	0.60m
Keel height 3	H_{k_3}	0.45m	0.50m
Outer wing thickness to chord ratio	$\frac{t}{c}_{out}$	10.7&	11.0%

Visually inspecting the planform, the first change that catches the eye is a larger inner wing and a smaller outer wing as compared to the baseline design. The increase in inner wing span distributes the weight of the payload over a larger percentage of the span, increasing the advantage inherent to flying wing concepts of locating weight close to the location of the lift. However, this means the outer wing decreases in size, with a shape otherwise very similar to the baseline.

The outer wing is used to house the elevons, as well as fulfilling a stabilising function similar to the horizontal tailplane of a conventional aircraft. Since the current study does not include stability and control considerations, further study is necessary to investigate whether this optimised outer wing geometry is sufficiently large to satisfy stability and controllability requirements.

The next difference is a slight decrease in sweep angle for the inner wing. The implications of this alteration are discussed in more detail in subsection 5.2.3, where the compressibility correction constraint is examined.

In addition to reduced sweep, the tapered rear part of the inner wing is slightly longer with more taper resulting in a narrower section at the end of the oval fuselage. Looking at Figure 5.3 we can see that the height of this section is similar to the baseline version, meaning the local thickness-to-chord ratio is larger at this point. The cross section of the inner part of the inner wing is quite similar in shape to the baseline version, albeit with a notably narrower cabin.

In order to accomodate the same payload as the baseline configuration, the narrower cabin of the optimised version is compensated by its length. A visualisation of the cabin layout is shown in Figure 5.4, adapted from Oosterom [22]. This alteration results in a 3-3-3 seat configuration in economy class instead of a 3-4-3 configuration, albeit with two extra rows of seats, resulting in a total of 1 extra seat per side of the V. This configuration places the seats at an angle of 18° to the flight direction, which is the maximum angle specified in CS25.785 [7]. This angled placement requires a stagger of the seats in order to obtain seat rows which are perpendicular to the cabin centreline, meaning slightly more width is necessary compared to conventional aircraft with similar seat configurations.

Looking at similar width cabins in current aircraft, the newest generation of Boeing's 777 aircraft manages to fit a 10-abreast configuration (3-4-3) in a cabin width of 5.96[2] which is only 2cm more than the optimised Flying V. Therefore, it is reasonable to expect that the optimised Flying V cabin with a width of 5.94m can accommodate the 9-abreast configuration shown, with the width of the extra seat in the 777 probably being taken up by the seat stagger.

[2] https://en.wikipedia.org/wiki/Boeing_777X

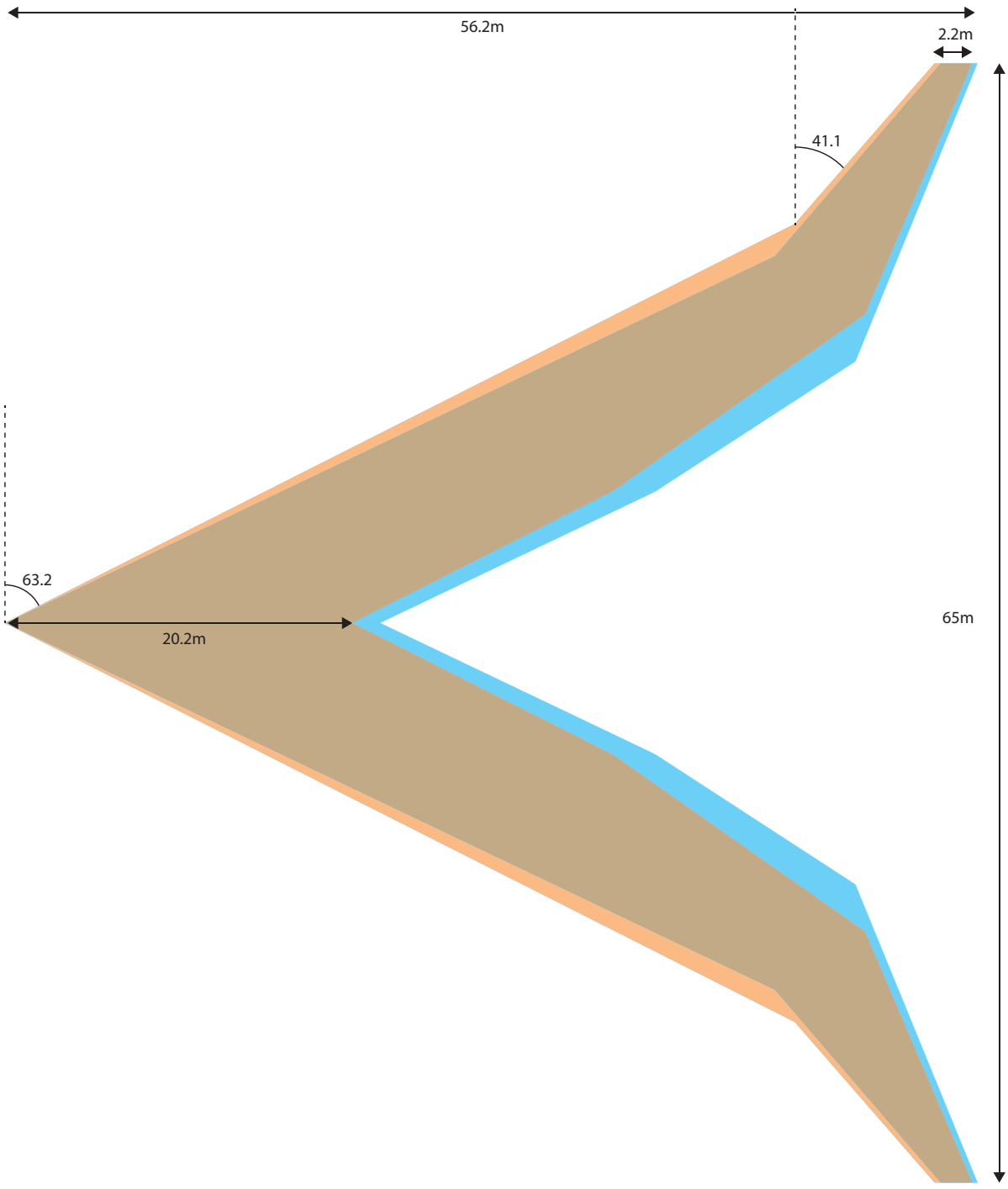

Figure 5.2: Optimised Flying V planform in orange, the baseline design in blue

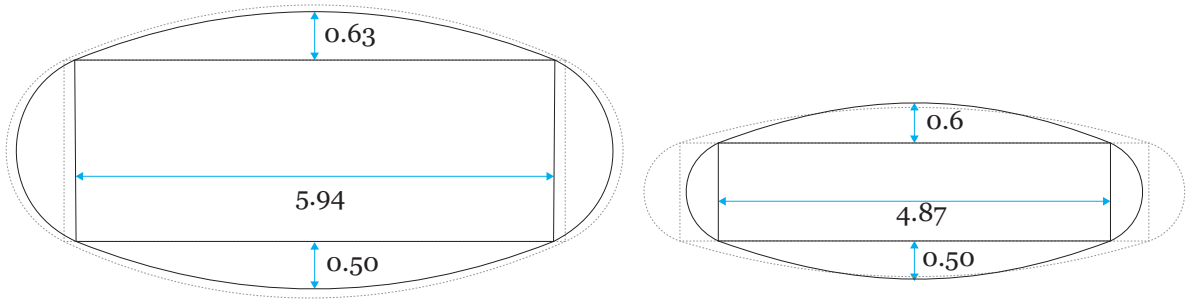

Figure 5.3: Cross sections at section 1 and 3, values in m. The baseline design is shown in dotted lines.

5.2.2. Performance Results

Key values for the optimised design are shown in Table 5.1 along with the conventional and baseline aircraft results. The payload-range diagram is shown in Figure 5.5, superimposed on the conventional aircraft data as published by Airbus for the A350-1000.

The optimised design results in a fuel burn which is 5 tonnes less than the baseline design, with an empty weight 11 tonnes lower. With regard to the conventional aircraft, this translates to a reduction in fuel burn of 35% with an MTOW reduction of 25%.

The wing planform area of the optimised configuration is lower than the baseline configuration, however, the wing loading is nearly identical since the total weight is lower. Compared to the conventional aircraft this wing loading is much lower, which is to be expected since the maximum lift coefficient of the Flying V is also lower due to the absence of HLDs and the limitation of the unstable pitch break.

The thrust-to-weight ratio is higher for the optimised variant than for the baseline variant, which is already higher than that of the conventional aircraft. This seems to indicate that a high thrust is necessary to meet the takeoff or one-engine-inoperative second segment climb gradient constraints, however, as will be discussed in the next section, this is not an active constraint. Therefore, further study is necessary to investigate whether a lower thrust-to-weight ratio is feasible for this configuration.

5.2.3. Constraints

For further development of the Flying V concept, it is interesting to know which aspects of the design limit the mission performance. Therefore, the compliance of the optimised result with the constraints is examined to find these aspects. The constraint compliance data is shown in Table 5.3.

Table 5.3: Constraint values

Constraint	Value	Requirement	Difference	Unit
Approach speed	140	147	-7	[kts]
Takeoff parameter	108	140	-32	$\left[\frac{kg^2}{m^2 N}\right]$
Cruise thrust	742	206	-536	[kN]
Climb gradient	3.1	2.4	-0.7	[%]
Cargo volume	255	250	-5	[m^2]
Cabin end ceiling height	2.15	1.9	-0.25	[m]
Fuel tanks volume	167	102	-65	[m^3]
$M^\star$ inner	0.92	0.91	0.01	[-]
$M^\star$ outer	0.93	0.93	0.0	[-]

As shown in the table, the values of $M^\star$ are very close to the requirement, meaning that both the inner and outer wing compressibility constraints are active, which indicates that the wave drag characteristics of both the inner and outer wings play a large role in the mission performance of the aircraft.

Since the method used in this study for compressibility drag does not adequately capture the complex dynamics which are at play in this consideration, further study is needed to investigate whether the sweep angle of the optimised configuration is feasible from an aerodynamic point of view. Specifically,

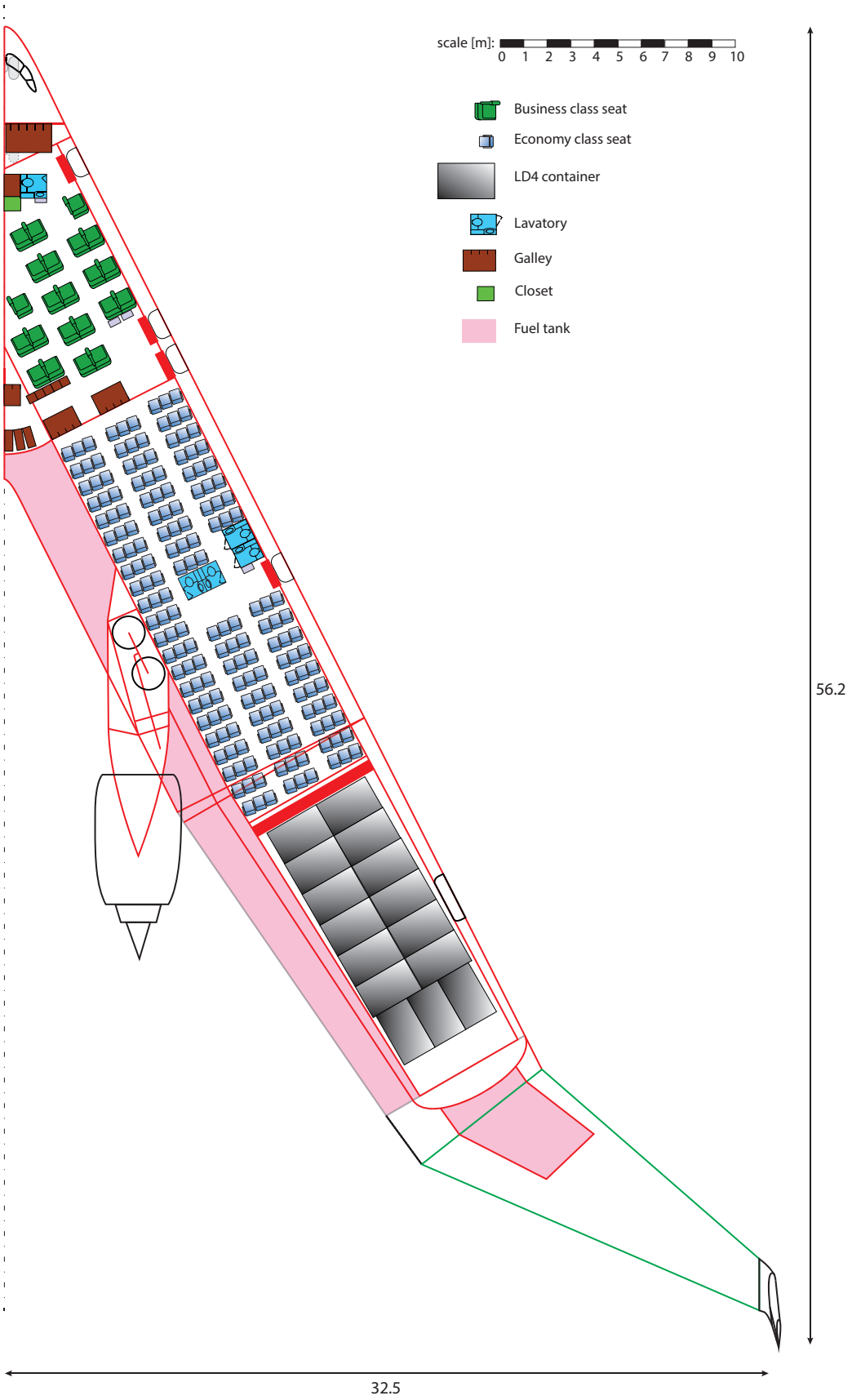

Figure 5.4: Interior layout for the newly optimised Flying V, adapted from [22]. Note that the cargo containers are indicative only, as the exact type of container to be used in the Flying V is not yet clear.

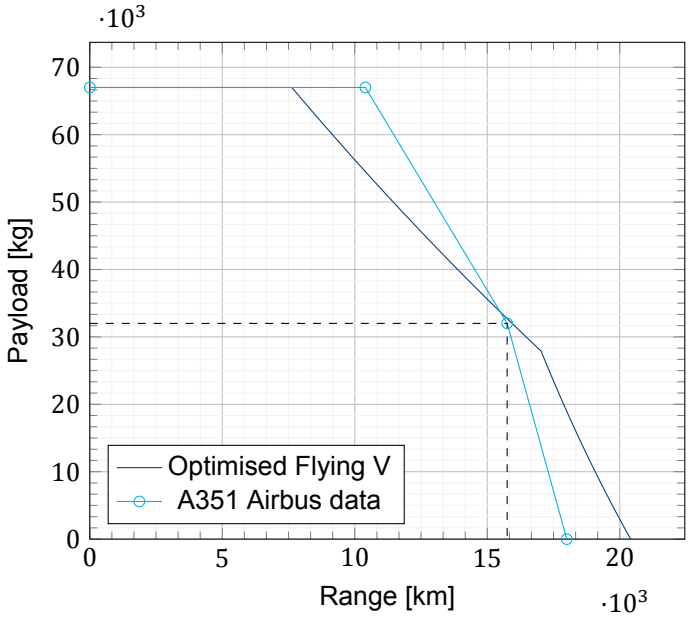

Figure 5.5: Payload-range diagram for the optimised Flying V-1000, compared to the Airbus A350-1000

since the method in this study is based on the lift coefficient of the entire inner or outer wing, local extremes are not taken into account. An area for which closer scrutiny in further investigation can prove useful is the end of the oval fuselage, which is expected to have a relatively high local lift coefficient due to the smaller chord. In combination with the relatively thick section this indicates that this section could require alteration to prevent excessive wave drag.

This matter also points to possible new research regarding the airfoil design of the inner wing. Better airfoil design may allow for the reduced sweep angle which, as shown by this optimisation, can play a role in further reducing the fuel used by this aircraft.

Finally, the fact that sweep plays an important role in efficiency may cause reevaluation of the proposed cruise Mach number since lower Mach numbers allow for lower sweep designs which are more efficient. This is, however, a discussion which must be conducted with many stakeholders, as both passengers and airlines may want to hold on to the current specification for time and operational reasons, while other stakeholders may value the efficiency and therefore environmental impact more.

Beside the compressibility constraint, no other constraints are near their value and therefore they are not active. As noted in subsection 5.2.2, the main driving requirements for thrust loading are usually the takeoff parameter and the second segment climb gradient constraints. However, these constraints are easily met by the optimised configuration, see Table 5.3. It should be noted that the method used for the second segment climb gradient in the current study gives an optimistic estimate, since the effect of the additional drag of the inoperational engine and the extra trim drag required in this assymetric scenario are not taken into account. Therefore, a more detailed analysis of this scenario should be part of further research to determine whether this configuration is feasible with lower thrust engines.

Finally, it is interesting to note that the fuel tank volume easily meets the requirements, having 65m^2 to spare. This could enable limiting the inboard tanks to only be placed outside the pressure cabin, reclaiming the volume between the trapezoid wall and the oval fuselage for systems, storage or additional cabin space.

6

Conclusions and Recommendations

The goals of the present study were to re-examine the Flying V on a conceptual level and to find possible improvements to the concept in terms of mission performance. This was achieved by developing an aircraft performance model for the Flying V and a conventional reference aircraft. This performance model was then integrated into an optimisation loop which optimised the conceptual design for a minimum mission fuel burn.

The analysed baseline design shows a considerable improvement over the conventional reference design, with a 31% reduction in fuel burn for the design mission at 21% lower maximum takeoff weight.

The optimised design further improves upon this result, showing a 35% reduction in mission fuel burn at 25% lower maximum takeoff weight. This was achieved by spreading the cabin and therefore inner wing out to an increased 71% of the span and decreasing the inner wing sweep angle to 63.2°. The increase in cabin span causes a narrower, longer cabin which moves more weight outboard, increasing the advantage flying wings have of placing weight where lift is produced to shorten load paths.

6.1. Conclusions

This study confirms the feasibility of a remarkable reduction in mission fuel burn aimed to be achieved by the Flying V concept. The mission performance for the Flying V was calculated, using an integration of results from previous analyses in an aircraft performance model. This resulted in 31% and 35% reduction in fuel burn with respect to a conventional aircraft for the baseline and optimised designs, respectively, which shows that the improvements in aerodynamic and structural efficiency achieved by this concept positively impact one another in a virtuous cycle to obtain a result which is greater than the sum of its parts.

The result of the optimisation based on the developed performance model shows several differences with respect to the baseline design, indicating possible improvements to the concept of the Flying V with respect to mission performance. The first difference is a change in division of the span between inner and outer wing, with a longer inner wing and a shorter outer wing. The improvement in mission performance shows that an improvement in wing loading and thus structure weight can be achieved by this alteration. However, this decrease in outer wing area resulting from the increase in inner wing span necessitates further research into the stability and control characteristics of the Flying V to determine whether acceptable performance is possible with this reduced outer wing size.

The second difference is a reduced sweep angle for the inner wing. Since the constraint on sweep angle to limit compressibility drag is active for both inner and outer wing, this shows that minimising the sweep is beneficial to the mission performance of the Flying V. Since the minimum feasible sweep is dependent on the thickness-to-chord ratio, airfoil technology, lift coefficient and Mach number, these are all factors which must be examined closely in further development of this concept.

6.2. Recommendations

This study confirms that the Flying V concept has a lot of potential to transform the long-range passenger aircraft market with its markedly reduced environmental impact. This section recommends several topics to investigate in the further development of this concept.

Firstly, the stability and control characteristics of the Flying V should be studied in more detail. This topic poses a challenge to designers of any flying wing, but for the Flying V specifically it is shown that reducing the size of the outer wing can result in an improvement in mission performance. Further research should therefore include an evaluation of the minimum size of the outer wings for which acceptable flight characteristics can be obtained.

Next, the high-subsonic aerodynamics of this concept warrant more study. The current study has shown that minimising the sweep angles of both the inner and outer wings can be beneficial to the mission performance. The interdependence of the airfoil characteristics with the cabin dimensions indicates a multidisciplinary tradeoff is to be made between the structural and aerodynamic disciplines. Specifically, a multidisciplinary study into the cross-section geometry of the inner wing seems promising since improvements in the airfoil geometry can enable a reduction in sweep angle, but is dependent on the limits of the oval fuselage and its structure. Additionally, the geometry at the transition between the inner and outer wings requires attention, both from an aerodynamic and from a structural standpoint since the currently used parameterisation does not provide a satisfactory geometry.

Finally, a stakeholder discussion regarding desirable cruise speed and hence cruise Mach numbers should be held to identify the relative values of travel time versus environmental impact, as these are shown to be opposing values. A model such as developed in this study, of low computational cost while describing the mission performance of an entire concept, can be employed to aid such a discussion. In this format, the traditional systems engineering procedure of defining requirements before starting the design engineering is revised to a process where these requirements can be weighed against important performance metrics.

Especially with increasing pressure on the environmental aspects of flying, this process allows for the evaluation of different solutions, such as propeller-based propulsion, which would otherwise not have been examined due to rigid requirements.

Bibliography

[1] Justus Benad. The Flying V - a new aircraft configuration for commercial passenger transport. In *Deutscher Luft- und Raumfahrtkongress*, Lilienthal-Oberth e.V., Bonn, 2015. Deutsche Gesellschaft für Luft- und Raumfahrt. URL https://publikationen.dglr.de/?tx_dglrpublications_pi1%5Bdocument_id%5D=370094.

[2] Shanling Yang, Mark Page, and Ed J. Smetak. *Achievement of NASA New Aviation Horizons N+2 Goals with a Blended-Wing-Body X-Plane Designed for the Regional Jet and Single-Aisle Jet Markets*. 2018. doi: 10.2514/6.2018-0521. URL https://arc.aiaa.org/doi/abs/10.2514/6.2018-0521.

[3] R. Martínez-Val. Conceptual design of a medium size flying wing. *Proceedings of the Institution of Mechanical Engineers, Part G: Journal of Aerospace Engineering*, 221(1):57, 2007. ISSN 2041-3025 0954-4100.

[4] Paul Okonkwo and Howard Smith. Review of evolving trends in blended wing body aircraft design. *Progress in Aerospace Sciences*, 82:1–23, 2016. ISSN 0376-0421. doi: 10.1016/j.paerosci.2015.12.002. URL https://dx.doi.org/10.1016/j.paerosci.2015.12.002.

[5] Zhenli Chen, Minghui Zhang, Yingchun Chen, Weimin Sang, Zhaoguang Tan, Dong Li, and Binqian Zhang. Assessment on critical technologies for conceptual design of blended-wing-body civil aircraft. *Chinese Journal of Aeronautics*, 32(8):1797–1827, 2019. ISSN 1000-9361. doi: 10.1016/j.cja.2019.06.006. URL https://dx.doi.org/10.1016/j.cja.2019.06.006.

[6] R. H. Liebeck. Design of the blended wing body subsonic transport. *Journal of Aircraft*, 41(1):10–25, 2004. ISSN 0021-8669. doi: 10.2514/1.9084. URL https://dx.doi.org/10.2514/1.9084.

[7] European Union Aviation Safety Agency. Cs-25 large aeroplanes, accessed on 21-07-2021. URL https://www.easa.europa.eu/certification-specifications/cs-25-large-aeroplanes.

[8] Sami Ammar, Clément Legros, and Jean-Yves Trépanier. Conceptual design, performance and stability analysis of a 200 passengers blended wing body aircraft. *Aerospace Science and Technology*, 71:325–336, 2017. ISSN 1270-9638. doi: 10.1016/j.ast.2017.09.037. URL https://dx.doi.org/10.1016/j.ast.2017.09.037.

[9] A. L. Bolsunovsky, N. P. Buzoverya, B. I. Gurevich, V. E. Denisov, A. I. Dunaevsky, L. M. Shkadov, O. V. Sonin, A. J. Udzhuhu, and J. P. Zhurihin. Flying wing—problems and decisions. *Aircraft Design*, 4(4):193–219, 2001. ISSN 1369-8869. doi: 10.1016/s1369-8869(01)00005-2. URL https://dx.doi.org/10.1016/S1369-8869(01)00005-2.

[10] R. Martinez-Val. Flying wings. a new paradigm for civil aviation? *Acta Polytechnica*, 47:32–43, 2007. doi: 10.14311/914. URL https://dx.doi.org/10.14311/914.

[11] R. Martinez-Val. Optimization of planform and cruise conditions of a transport flying wing. *Proceedings of the Institution of Mechanical Engineers, Part G: Journal of Aerospace Engineering*, 224(12):1243, 2010. ISSN 2041-3025 0954-4100.

[12] John H. McMasters and Ilan M. Kroo. Advanced configurations for very large transport airplanes. *Aircraft Design*, 1(4):217–242, 1998. ISSN 1369-8869. doi: 10.1016/s1369-8869(98)00018-4. URL https://dx.doi.org/10.1016/S1369-8869(98)00018-4.

[13] John T. Bonet, Harvey G. Schellenger, Blaine K. Rawdon, Kevin R. Elmer, Sean R. Wakayama, Derrell L. Brown, and Yueping Guo. Environmentally responsible aviation (era) project - n+2 advanced vehicle concepts study and conceptual design of subscale test vehicle (stv) final report.

Report NASA/CR-2011-216519, DFRC-E-DAA-TN8572, NASA Dryden Flight Research Center; Edwards, CA United States, 11-12-2011 2011. URL https://ntrs.nasa.gov/search.jsp?R=20140005559.

[14] P. Panagiotou, S. Fotiadis-Karras, and K. Yakinthos. Conceptual design of a blended wing body male uav. *Aerospace Science and Technology*, 73:32–47, 2018. ISSN 1270-9638. doi: 10.1016/j.ast.2017.11.032. URL https://dx.doi.org/10.1016/j.ast.2017.11.032.

[15] Francesco Faggiano, Roelof Vos, Max Baan, and Reinier Van Dijk. Aerodynamic design of a flying v aircraft. American Institute of Aeronautics and Astronautics, 2017. doi: 10.2514/6.2017-3589. URL https://dx.doi.org/10.2514/6.2017-3589.

[16] R. Vos, F. J. J. M. M. Geuskens, and M. F. M. Hoogreef. A new structural design concept for blended wing body cabins. American Institute of Aeronautics and Astronautics. doi: 10.2514/6.2012-1998. URL https://dx.doi.org/10.2514/6.2012-1998.

[17] Rob Viet. *Analysis of the flight characteristics of a highly swept cranked flying wing by means of an experimental test*. Thesis, 2019. URL http://resolver.tudelft.nl/uuid:90de4d9e-70ae-4efc-bd0a-7426a0a669c3.

[18] Berta Rubio Pascual. *Engine-Airframe Integration for the Flying V*. Thesis, 2018. URL http://resolver.tudelft.nl/uuid:75be27a7-6fd4-4112-a600-45df2999758f.

[19] Alberto Ruiz García. *Aerodynamic Model Identification of the Flying V from Wind Tunnel Data*. Thesis, 2019. URL http://resolver.tudelft.nl/uuid:79e01f29-1789-4501-8556-ca2bcf06f3ab.

[20] Ankith J. Santosh. *Influence of Ground Effect on the Flying V aircraft*. Thesis, 2020. URL http://resolver.tudelft.nl/uuid:d34e14b2-fed5-4e4f-a448-aa0fb92e0331.

[21] Marco Palermo. *The Longitudinal Static Stability and Control Characteristics of a Flying V Scaled Model*. Thesis, 2019. URL http://resolver.tudelft.nl/uuid:6286f9e2-c24a-430c-a4fa-9fb67b9558b4.

[22] Wilco Oosterom. *Flying-V Family Design*. Thesis, 2021. URL http://resolver.tudelft.nl/uuid:9e8f9a41-8830-405d-8676-c46bf6b07891.

[23] Nelson Johnson. *Effect of Winglet Integration and Rudder Deflection on Flying-V Aerodynamic Characteristics*. Thesis, 2021. URL http://resolver.tudelft.nl/uuid:b664ae03-846f-4ad3-849a-c081a32260ad.

[24] Jackson Horwitz. *Parametric Design of the Flying-V Winglets for Improved Lateral-Directional Stability and Control*. Thesis, 2021. URL http://resolver.tudelft.nl/uuid:d7513b36-b9fd-4f8a-8726-f5c7ee7f3a6b.

[25] Grégoire Bourget. *The effect of landing gear implementation on Flying V aerodynamics, stability and controllability*. Thesis, 2020. URL http://resolver.tudelft.nl/uuid:599eca91-6200-4d29-8dd7-e4e7060703e1.

[26] Ricardo van der Pluijm. *Cockpit Design and Integration into the Flying V*. Thesis, 2021. URL http://resolver.tudelft.nl/uuid:da4a8d74-32fa-45f1-9f92-d01d45fdea01.

[27] Francesco Faggiano. *Aerodynamic Design Optimization of a Flying V Aircraft*. Thesis, 2016. URL http://resolver.tudelft.nl/uuid:0b1472a5-3aad-433c-9a64-242c84b114fd.

[28] Jeroen Van Uitert. *Experimental Investigation into the Effect of Aerodynamic Add-ons on the Aerodynamic Characteristics of the Flying V*. Thesis, 2021. URL http://resolver.tudelft.nl/uuid:fdfff622-792c-4d54-a048-b59abf477a11.

[29] John Vassberg, Mark Dehaan, Melissa Rivers, and Richard Wahls. Development of a common research model for applied cfd validation studies. American Institute of Aeronautics and Astronautics, 2008. doi: 10.2514/6.2008-6919. URL https://dx.doi.org/10.2514/6.2008-6919.

[30] L.A. van der Schaft. *Development, Model Generation and Analysis of a Flying V Structure Concept*. Thesis, 2017. URL http://resolver.tudelft.nl/uuid:d9c9c02f-d67a-4e3c-93a7-eb20ed67cd03.

[31] Mathias Claeys. *Flying V and Reference Aircraft Structural Analysis and Mass Comparison*. Thesis, 2018. URL http://resolver.tudelft.nl/uuid:ee7f2ecb-cdb6-46de-8b57-d55b89f8c7e6.

[32] E. Torenbeek. *Synthesis of Subsonic Airplane Design*. Delft University Press and Kluwer Academic Publishers, Delft and Dordrecht, 1982. ISBN 90-247-2724-3.

[33] Jr. Anderson, John D. *Fundamentals of aerodynamics*. Anderson series. McGraw-Hill, New York, fifth edition. edition, 2011. ISBN 9780073398105 0073398101 9780071289085 0071289089.

[34] Brandon Basgall, Wanbo Liu, Truman Cassady, and Willem A. Anemaat. Aircraft design weight methods comparison and improvement, 6-10 January 2020 2020. URL https://doi-org.tudelft.idm.oclc.org/10.2514/6.2020-1259.

[35] J. Roskam. *Airplane Design Part V: Component Weight Estimation*, volume 5 of *Airplane Design*. Roskam Aviation and Engineering Corporation, Ottawa, 1985.

[36] John William Ransom Taylor and Kenneth Munson. *Jane's all the world's aircraft*. Jane's Pub., London, New York, 1985.

[37] M Droegkamp. 2089. finite element model weight estimation, 5-18-1992 1992. URL https://www.sawe.org/papers/2089/buy.

[38] Mark Drela. *Integrated simulation model for preliminary aerodynamic, structural, and control-law design of aircraft*. 1999. doi: 10.2514/6.1999-1394. URL https://arc.aiaa.org/doi/abs/10.2514/6.1999-1394.

[39] Egbert Torenbeek. *Advanced Aircraft Design : Conceptual Design, Analysis andOptimization of Subsonic Civil Airplanes*. John Wiley & Sons, Incorporated, New York, UNITED KINGDOM, 2013. ISBN 9781118568088. URL http://ebookcentral.proquest.com/lib/delft/detail.action?docID=1184219.

[40] Ed Obert, Ronald Slingerland, Debbie J. W. Leusink, Tobie van den Berg, Justin H. Koning, and M. J. L. van Tooren. *Aerodynamic design of transport aircraft*. I.O.S. Press, Amsterdam, 2009. ISBN 978-1-58603-970-7.

[41] Sighard F. Hoerner. *Fluid-dynamic drag : practical information on aerodynamic drag and hydrodynamic resistance*. Hoerner Fluid Dynamics, Bakersfield, 2nd ed. edition, 1992. ISBN 9991194444 9789991194448.

[42] Daniel P. Raymer, Aeronautics American Institute of, and Astronautics. *Aircraft design : a conceptual approach*. AIAA education series. American Institute of Aeronautics and Astronautics, Reston, VA, 5th ed. edition, 2012. ISBN 9781600869112 1600869114.

[43] J. Roskam. *Airplane Design Part I: Preliminary sizing of airplanes*, volume 1 of *Airplane Design*. Roskam Aviation and Engineering Corporation, Ottawa, 1985. ISBN 9781884885426.

[44] Rainer Storn and Kenneth Price. Differential evolution - a simple and efficient heuristic for global optimization over continuous spaces. *Journal of Global Optimization*, 11:341–359, 01 1997. doi: 10.1023/A:1008202821328.

[45] Pauli Virtanen, Ralf Gommers, Travis E. Oliphant, Matt Haberland, Tyler Reddy, David Cournapeau, Evgeni Burovski, Pearu Peterson, Warren Weckesser, Jonathan Bright, Stéfan J. van der Walt, Matthew Brett, Joshua Wilson, K. Jarrod Millman, Nikolay Mayorov, Andrew R. J. Nelson, Eric Jones, Robert Kern, Eric Larson, C J Carey, İlhan Polat, Yu Feng, Eric W. Moore, Jake VanderPlas, Denis Laxalde, Josef Perktold, Robert Cimrman, Ian Henriksen, E. A. Quintero, Charles R. Harris, Anne M. Archibald, Antônio H. Ribeiro, Fabian Pedregosa, Paul van Mulbregt, and SciPy 1.0 Contributors. SciPy 1.0: Fundamental Algorithms for Scientific Computing in Python. *Nature Methods*, 17:261–272, 2020. doi: 10.1038/s41592-019-0686-2.

[46] Pieter-Jan Proesmans and Roelof Vos. Airplane design optimization for minimal global warming impact. American Institute of Aeronautics and Astronautics, 2021. doi: 10.2514/6.2021-1297. URL https://dx.doi.org/10.2514/6.2021-1297.

[47] Airbus S.A.S. Aircraft characteristics airport and maintenance planning, July 2021. URL https://www.airbus.com/aircraft/support-services/airport-operations-and-technical-data/aircraft-characteristics.html.

[48] Melissa Rivers and Ashley Dittberner. *Experimental Investigations of the NASA Common Research Model in the NASA Langley National Transonic Facility and NASA Ames 11-Ft Transonic Wind Tunnel (Invited)*. 2011. doi: 10.2514/6.2011-1126. URL https://arc.aiaa.org/doi/abs/10.2514/6.2011-1126.

[49] Marleen Hillen. *Parametrisation of the Flying-V Outer Mould Line*. Thesis, 2020. URL http://resolver.tudelft.nl/uuid:f4863ae4-2792-4335-b929-ff9dfdb6fed5.

[50] R. K. Nangia. Efficiency parameters for modern commercial aircraft. 110(1110):495–510, 2006. ISSN 0001-9240. doi: 10.1017/s0001924000001391. URL https://dx.doi.org/10.1017/s0001924000001391.

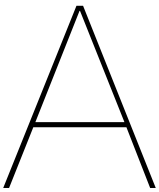

Conventional Aircraft Inputs

This appendix contains a listing of the inputs used in the conventional aircraft model based on the Airbus A350, for both the -900 and -1000 variants.

Table A.1: Inputs for the A350-900 aircraft model. *Value with an asterisk for the extra long range variant

Parameter	Symbol	Value	Unit
Wing			
Span	b	64.75	m
Leading Edge Sweep	Λ_{LE}	35	°
Half Chord Sweep	$\Lambda_{\frac{1}{2}\text{c}}$	30.5	°
Taper	λ	0.159	-
Area	S	439	m^2
Root thickness-to-chord ratio	$\frac{t}{c}_{\text{r}}$	0.15	-
Aspect Ratio	A	9.55	-
Wetted Area	S_{w}	763	m^2
Mean Aerodynamic Chord	MAC	7.38	m
Average thickness-to-chord ratio	$\frac{t}{c}_{\text{avg}}$	0.1	-
Flap			
Leading Edge Sweep	Λ_{f}	14.1	°
Thickness-to-chord ratio	$\frac{t}{c}_{\text{f}}$	0.15	-
Area	S_{f}	60	m^2
Structural span	b_{fs}	41.6	m
Maximum Deflection	δ_{f}	39	°
Slat			
Area	S_{lef}	37	m^2
Empennage			
Horizontal Stabiliser Area	S_{h}	83	m^2
Vertical Stabiliser Area	S_{v}	62	m^2
Thickness-to-chord ratio	$\frac{t}{c}_{\text{emp}}$	0.12	-
Mean Aerodynamic Chord	MAC_{emp}	4.8	m
Fuselage			
Width	b_{f}	5.96	m
Height	h_{f}	6.09	m
Length	l_{f}	65.3	m
Tail length	l_{t}	34	m
Gross Shell Area	S_{G}	1073	m^2
Passenger cabin length	l_{pc}	52	m
Engine			
Takeoff thrust per engine	T_{TO}	375	kN
Nacelle width	b_{n}	3.9	m
Nacelle length	l_{n}	6.4	m
Nacelle wetted area	$S_{\text{w}_{\text{n}}}$	68.5	m^2
Pylon width	b_{p}	1.6	m
Pylon length	l_{p}	11.1	m
Pylon wetted area	$S_{\text{w}_{\text{p}}}$	32.3	m^2
Systems			
Fuel tank volume	V_{fuel}	140.8/166.5*	m^3
Electric power	P_{el}	400	kVA
Miscellaneous			
Flight crew	N_{fc}	4	-
Cabin crew	N_{cc}	8	-
Passengers (typical)	N_{pax}	315	-
of which business	$N_{\text{pax}_{\text{b}}}$	48	-
Passengers (maximum)	$N_{\text{pax}_{\text{max}}}$	440	-
Maximum payload	$w_{\text{PL}_{\text{max}}}$	53	$\cdot 10^3$ kg

Table A.2: Inputs for the A350-1000 aircraft model

Parameter	Symbol	Value	Unit
Wing			
Span	b	64.75	m
Leading Edge Sweep	Λ_{LE}	35	°
Half Chord Sweep	$\Lambda_{\frac{1}{2}\text{c}}$	30.5	°
Taper	λ	0.159	-
Area	S	460	m^2
Root thickness-to-chord ratio	$\frac{t}{c}_{\text{r}}$	0.15	-
Aspect Ratio	A	9.55	-
Wetted Area	S_{w}	799	m^2
Mean Aerodynamic Chord	MAC	7.38	m
Average thickness-to-chord ratio	$\frac{t}{c}_{\text{avg}}$	0.1	-
Flap			
Leading Edge Sweep	Λ_{f}	14.1	°
Thickness-to-chord ratio	$\frac{t}{c}_{\text{f}}$	0.15	-
Area	S_{f}	60	m^2
Structural span	b_{fs}	41.6	m
Maximum Deflection	δ_{f}	39	°
Slat			
Area	S_{lef}	37	m^2
Empennage			
Horizontal Stabiliser Area	S_{h}	83	m^2
Vertical Stabiliser Area	S_{v}	62	m^2
Thickness-to-chord ratio	$\frac{t}{c}_{\text{emp}}$	0.12	-
Mean Aerodynamic Chord	MAC_{emp}	4.8	m
Fuselage			
Width	b_{f}	5.96	m
Height	h_{f}	6.09	m
Length	l_{f}	72.3	m
Tail length	l_{t}	37	m
Gross Shell Area	S_{G}	1187	m^2
Passenger cabin length	l_{pc}	56	m
Engine			
Takeoff thrust per engine	T_{TO}	432	kN
Nacelle width	b_{n}	3.9	m
Nacelle length	l_{n}	6.4	m
Nacelle wetted area	$S_{\text{w}_{\text{n}}}$	68.5	m^2
Pylon width	b_{p}	1.6	m
Pylon length	l_{p}	11.1	m
Pylon wetted area	$S_{\text{w}_{\text{p}}}$	32.3	m^2
Systems			
Fuel tank volume	V_{fuel}	158.8	m^3
Electric power	P_{el}	400	kVA
Miscellaneous			
Flight crew	N_{fc}	4	-
Cabin crew	N_{cc}	12	-
Passengers (typical)	N_{pax}	369	-
of which business	$N_{\text{pax}_{\text{b}}}$	54	-
Passengers (maximum)	$N_{\text{pax}_{\text{max}}}$	480	-
Maximum payload	$w_{\text{PL}_{\text{max}}}$	67	$\cdot 10^3$ kg